Structural Variation Along the Southern Hikurangi Subduction Zone, Aotearoa New Zealand, From Seismic Reflection and Retro-Deformation Analysis

D. E. Stevens[1,2] , L. C. McNeill[1] , T. J. Henstock[1] , P. M. Barnes[3] , G. Crutchley[3,4] , N. Bangs[5] , S. Henrys[6] , and H. J. A. Van Avendonk[5]

[1]School of Ocean and Earth Science, University of Southampton, Southampton, UK, [2]British Geological Survey, The Lyell Centre, Edinburgh, UK, [3]National Institute of Water and Atmospheric Research (NIWA), Wellington, New Zealand, [4]GEOMAR Helmholtz Centre for Ocean Research Kiel, Kiel, Germany, [5]Institute for Geophysics, University of Texas, Austin, TX, USA, [6]GNS Science, Lower Hutt, New Zealand

Abstract The southern Hikurangi subduction zone exhibits significant along-strike variation in convergence rate and obliquity, sediment thickness and, uniquely, the increasing proximity of southern Hikurangi to, and impingement on, the incoming continental Chatham Rise, an ancient Gondwana accretionary complex. There are corresponding changes in the morphology and structure of the Hikurangi accretionary prism. We combine widely spaced multichannel seismic reflection profiles with high resolution bathymetry and previous interpretations to characterize the structure and the history of the accretionary prism since 2 Ma. The southern Hikurangi margin can be divided into three segments. A northeastern segment (A) characterized by a moderately wide (∼70 km), low taper (∼5°) prism recording uninhibited outward growth in the last ∼1 Myr. Deformation resolvable in seismic reflection data accounts for ∼20 % of plate convergence, comparable with the central Hikurangi margin further North. A central segment (B) characterized by a narrow (∼30 km), moderate taper (∼8°) prism, with earlier (∼2-∼1 Ma) shortening than segment A. Outward prism growth ceased coincidentally with development of major strike-slip faults in the prism interior, reduced margin-normal convergence rate, and the onset of impingement on the incoming Chatham Rise to the south. A southwestern segment (C) marks the approximate southern termination of subduction but widens to ∼50 km due to rapid outward migration of the deformation front via fault reactivation within the now-underthrusting corner of the Chatham Rise. Segment C exhibits minimal shortening as margin-normal subduction velocity decreases and plate motion is increasingly taken up by interior thrusts and strike-slip faults.

Plain Language Summary Between the North and South Islands of New Zealand, the interaction of the Pacific and Australian tectonic plates is highly complex. Beneath the North Island, the Pacific plate moves westward and slides underneath the Australian plate at the Hikurangi subduction zone, but through the South Island, the two plates slide past each other along the Alpine Fault. The transition between these two zones affects tectonic patterns to the north and south, and the resulting earthquake and tsunami hazard. Using marine seismic reflection technology, we have built detailed cross-sectional images of the shallowest ∼20 km of the structure of the Earth beneath the seabed, which record the history of plate interactions. By studying how the structure changes from northeast to southwest off the east coast of New Zealand, we can link these changes to tectonic processes. We suggest that changes in fault structure and activity relate to relatively low-density rocks off the east coast of New Zealand. These lower density rocks were formed during a now extinct phase of tectonic activity, but in the present day they are impinging on the Hikurangi subduction zone. This changes the relative buoyancy of the two tectonic plates and inhibits subduction.

1. Introduction

Subduction zone forearcs are areas of significant geological structural complexity. At subduction margins with a thick column of incoming sediment, the frontal accretionary prism is composed of ocean-derived sediments from the oceanic plate, as well as material recycled from the upper plate via gravity-driven mass-wasting and subsequent accretion (von Huene et al., 2009). Therefore, the outermost prism is usually composed of poorly consolidated, fluid-rich material, creating an environment which promotes velocity-strengthening seismic behavior and deforms easily (Kopp, 2013; Moore & Saffer, 2001). The outermost prism is therefore the part of a

Supervision: L. C. McNeill,
T. J. Henstock, N. Bangs
Validation: P. M. Barnes, G. Crutchley,
N. Bangs
Visualization: D. E. Stevens
Writing – original draft: D. E. Stevens
Writing – review & editing:
D. E. Stevens, L. C. McNeill,
T. J. Henstock, P. M. Barnes, G. Crutchley,
N. Bangs, S. Henrys,
H. J. A. Van Avendonk

subduction zone which is most sensitive to changes in boundary conditions, resulting in structural variation, for example, changes in thrust fault vergence (Dominguez et al., 1998; Lallemand et al., 1992).

Prism structure at accretionary margins usually consists of a sequence of landward dipping thrusts, forming seaward-vergent fault-propagation-folds, where contemporary strain is often concentrated at the outermost (furthest seaward) fault (e.g., Ellis et al., 2019; Moore et al., 2009; Smith et al., 2012). Thrust faults within older parts of the prism may remain continuously active or have initiated/propagated landward of the deformation front, or become reactivated. Here we refer to thrusts as being out-of-sequence where they initiate within older parts of the prism landward of the frontal thrust. We also highlight structures landward of the frontal thrust along which there has been continued activity (but these are not considered as out-of-sequence). Further structural complexity is exhibited by some margins, where seaward dipping thrusts form landward-vergent folds, either throughout or in parts of the prism (where "mixed" vergence includes both fault geometries). Prime examples of margins which exhibit mixed vergence include Cascadia (Gulick et al., 1998; MacKay et al., 1992) and Sumatra (McNeill & Henstock, 2014; Moeremans et al., 2014).

Detailed analysis of the variation in prism structure at accretionary margins can also help to link structural configuration (fault geometry, density, activity and strain) to characteristics of the incoming plate, such as sediment thickness and properties, seafloor or basement rugosity, and convergence obliquity, which may act as controls on the prism structure (Cook et al., 2014; McNeill & Henstock, 2014). Studies using 2D seismic reflection data have shown that prism structure can change rapidly along strike (MacKay et al., 1992; Smith et al., 2012). Structural variation has previously been linked to: topography of the incoming oceanic basement (McNeill & Henstock, 2014; Pedley et al., 2010); thickness of the incoming sediment (von Huene & Scholl, 1991; Wallace et al., 2009; Heuret et al., 2012; Cook et al., 2014; McNeill & Henstock, 2014) and temporal variations in how much sediment is either accreted, subducted or underplated (Clift & Vannucchi, 2004); the degree of plate convergence obliquity and the rate of orthogonal convergence (Clift & Vannucchi, 2004; McNeill & Henstock, 2014); the dip angle of the subducting plate; and the physical properties along the plate interface, which control the basal shear stress and the slope angle of the outer prism (Davis et al., 1983; Saffer & Bekins, 2002).

Abrupt along-strike changes in prism structure, which can be deduced from geophysical data, may be linked to terminations of megathrust earthquake rupture segments (Kopp et al., 2008; McNeill & Henstock, 2014), and to differences in seismogenic and tsunamigenic potential (Cook et al., 2014; Kopp, 2013). In addition, tsunami risk may be enhanced by out-of-sequence faulting or major active faults further inboard in the forearc (Bangs et al., 2009). These faults may splay from the plate interface at depth, intercept the seafloor, and be set within cohesively strong parts of the prism. Therefore, where such faults are active or prone to reactivation, they may generate co-seismic seafloor uplift, posing an important mechanism in tsunamigenesis (Collot et al., 2004; Sibuet et al., 2007).

Structural information deduced from seismic reflection data can also be used to estimate the sequence of thrust fault activation, and therefore assess the temporal evolution of internal deformation within accretionary prisms. Deformed prism geological structure interpreted from seismic profiles across the subduction zone, and sub-parallel to the orthogonal vector of plate convergence, can be restored to a pre-deformed state to evaluate timing and rates of tectonic shortening, and therefore strain distribution through time (Boston et al., 2016; Ghisetti et al., 2016; Lackey et al., 2020; Moore et al., 2011). Although the results are non-unique and therefore do not represent a precise history of the accretionary prism, these techniques can be used to infer geologically reasonable deformation pathways (Hossack, 1979). Progressive restoration, where the sequence of deformation is determined from the occurrence of growth strata in the hanging walls of fault-propagation folds and a reliable chronostratigraphy, thus provides a useful tool to compare relative differences in compressional strain rate along-strike (Ghisetti et al., 2016).

In this study, we present new interpretations of three multichannel seismic reflection profiles that image the outer accretionary prism and part of the incoming plate at the southern Hikurangi subduction margin, updating interpretations by Bland et al. (2015). Using the correlatable seismic stratigraphy originally defined by Barnes et al. (2010) we use our interpretation to identify distinct structural segments along the margin, reconstruct the structural evolution of the southern Hikurangi prism since 2 Ma, and determine the outward propagation rate of the deformation front. We combined our interpretation with previous interpretations of regional structure (Barnes et al., 2010; Crutchley et al., 2020; Ghisetti et al., 2016; Micallef et al., 2014; Mountjoy et al., 2009; Wallace, Barnes, et al., 2012) and with information about the incoming plate such as along-strike changes in margin-

normal velocity (Wallace et al., 2018), sediment thickness, and morphology to identify along-strike differences in the deformation of the prism distinct enough to be classed as separate structural segments.

2. Tectonic Setting

The Hikurangi subduction margin is located off the east coast of New Zealand's North Island (Figure 1). The westward subduction of the Pacific Plate beneath the Australian Plate (and New Zealand's continental crust) initiated ca. 24–30 Ma (Ballance, 1976; Rait et al., 1991; Stern et al., 2006). The incoming Pacific Plate crust in this region is composed of the Hikurangi Plateau, an oceanic Large Igneous Province formed ca. 120 Ma (Davy et al., 2008). During the late Early Cretaceous, part of the Hikurangi Plateau was subducted at the Gondwana subduction margin (Davy et al., 2008; Strogen et al., 2022), beneath what is today the east-west striking Chatham Rise, a component of the Mesozoic accretionary prism (Riefstahl et al., 2020). Subduction ceased along this section of the Gondwana margin when the subduction system was choked by convergence of the thick, buoyant, crust of the Hikurangi Plateau (Wood & Davy, 1994).

The modern-day Hikurangi margin exhibits a range of significant changes along-strike from north to south. The present-day relative motion rate between the Pacific and Australian plates offshore New Zealand's North Island is 33–48 mm/yr (Beavan et al., 2002), but due to the tectonic rotation of the North Island, the direction and magnitude of relative plate motion varies substantially (Wallace, Barnes, et al., 2012). At the northern end of the North Island (38°–40°S) convergence is slightly oblique (~30° from perpendicular to the deformation front) and the Australian-Pacific relative plate motion rate at the trench (margin-normal subduction velocity) is ~50 mm/yr (Wallace et al., 2018). There is a progressive southward decrease in subduction velocity accompanying the substantial increase in obliquity (Figure 1b). Between 38°S and 41.5°S this change is gradual, ultimately resulting in highly oblique convergence (~60°) and reduced margin-normal subduction velocity (~25–35 mm/yr) (Wallace et al., 2018; Figure 1b). Southeast of Cook Strait, relative plate motion is near margin-parallel due to a change in orientation of the plate boundary (from south-south-west to south-west/west-south-west) and a simultaneous change in the Pacific Plate motion vector from ~west to west-south-west (Barnes et al., 1998; Wallace, Barnes, et al., 2012). This results in an abrupt decrease in margin-normal subduction velocity to less than 7 mm/yr at ~42°S (Wallace et al., 2018; Figure 1b). These changes are summarized in Figure 1 and Table 1. Between the North and South Islands there is a transition from subduction to strike-slip/transpressional tectonics, and in north-eastern South Island a large proportion of the relative plate motion is accommodated by dextral strike-slip faults of the Marlborough Fault Zone (Wallace, Barnes, et al., 2012). Partitioning of strike-slip and convergent components of the overall plate motion in this transition zone extends offshore. The Boo-Boo Fault in Cook Straight, which strikes approximately parallel to Pacific Plate motion, has a slip rate of ~8 mm/yr and is thought to accommodate ~20% of plate motion (Seebeck et al., 2023).

There is also substantial north-south variation in the morphology, sediment thickness and composition of the incoming Pacific Plate. The northern part of the Hikurangi margin is characterized by an incoming oceanic plate (Hikurangi Plateau) studded with numerous seamounts, creating rough topography (Barker et al., 2009; Barnes et al., 2020; Bell et al., 2010; Pedley et al., 2010). Axial trench sediments in the Hikurangi Trough, forming the trench wedge, onlap onto the Hikurangi Plateau in the North, and onto the Chatham Rise in the south. The total sediment thickness on the incoming plate, including the siliciclastic trench wedge and the underlying Hikurangi Plateau cover sequences, increases from ~1.0 to 1.5 km in the north, to a maximum of 9 km in the south (Lewis et al., 1998; Plaza-Faverola et al., 2012). Input sediments to the northern Hikurangi subduction zone have been recently sampled by International Ocean Discovery Program (IODP) Expeditions 372B and 375 at Site U1520 (Wallace et al., 2019). The trench wedge sediments are composed mostly of turbidite sands and silts, and hemipelagic muds. The underlying Hikurangi Plateau cover sequence includes marls, carbonates, thin tephra layers, and volcaniclastic conglomerates. However, the IODP sample sites are significantly north of our study area and have not yet been tied to seismic data in the south.

There are differences in the subduction interface slip behavior between northern and southern parts of the margin, including in the area of this study. In the north, offshore Gisborne, shallow (<15 km) slow slip events (SSEs) occur on the plate interface (Wallace, Beavan, et al., 2012). In the south, SSEs occur much deeper (25–40 km) (Bartlow et al., 2014; Wallace & Beavan, 2010; Wallace, Beavan, et al., 2012, 2018). From GPS velocities and active fault slip data, Wallace, Barnes, et al. (2012) developed a model of slip rate deficit on the subducting plate interface (Wallace et al., 2004, 2007), where high slip rate deficits (>20 mm/yr) correlate with a high degree of
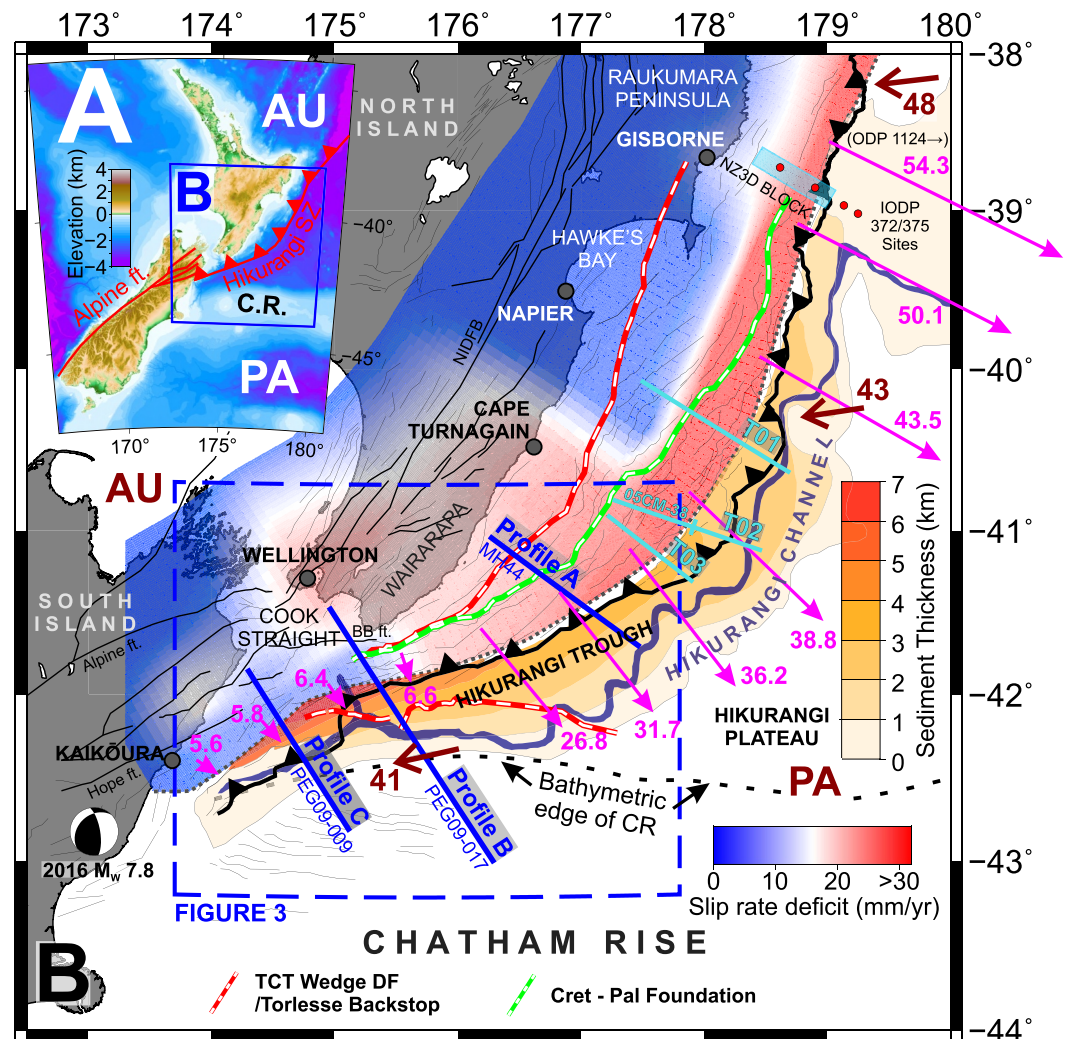
Figure 1. (a) Tectonic setting of New Zealand showing the area expanded in (b). PA is the Pacific Plate, which subducts beneath the Australian Plate (AU) at the Hikurangi subduction zone. (b) Tectonic environment and locations of our seismic profiles (thick blue lines). Thick light-blue lines are location of seismic profiles T01, T02 (a composite profile that includes line 05CM-38 from Barker et al. (2009)), and T03 from Ghisetti et al. (2016). Thin black lines are faults; heavy toothed black line indicates the Hikurangi subduction zone deformation front as mapped by the NZCFM (Seebeck et al., 2023); Dark red arrows are motion vectors (mm/yr) for the Pacific Plate relative to the Australian Plate from Beavan et al. (2002) and magenta arrows are motion vectors of the overriding plate relative to the Pacific Plate at the Hikurangi trench (margin-normal subduction velocities) from Wallace et al. (2018), both in mm/year. Siliclastic trench wedge sediment thicknesses above Reflector R5B (see Figure 2) are from Lewis et al. (1998). Slip rate deficit grid from Wallace, Barnes, et al. (2012),—see color bar in bottom-right of figure (sediment thickness polygons and slip rate deficit grid separated by dotted gray line). Beach ball indicates epicenter location and focal mechanism of the 2016 Kaikōura earthquake (Hamling et al., 2017). Red dots indicate locations of the IODP Expedition 372/375 boreholes (Wallace et al., 2019) and light blue shaded area indicates the location of the 3D seismic volume acquired by the NZ3D experiment (MGL1801 participants, 2018). The green and white dashed line is the boundary between the buried Late Cretaceous-Palaeogene passive margin foundation and the Late Cenozoic frontal accretionary prism (Barnes et al., 2010; Bassett et al., 2022; Gase et al., 2021). The red and white dashed lines are the buried updip extent of the Mesozoic Torlesse Composite Terrane (TCT) thrust wedge striking (1) north-east close to the North Island coastline (from Bassett et al., 2022) (referred to as the Wairarapa TCT Backstop); and (2) E-W along the northern Chatham Rise (mapped as part of this, and upcoming studies, using a compilation of seismic reflection data), (referred to as the Chatham Rise TCT Wedge Deformation Front). BB ft. = Boo-Boo Fault.

interseismic coupling. Plate coupling varies greatly along the margin, with a distinct transition between strong and weak coupling occurring around 40°S (Figure 1; Wallace, Barnes, et al., 2012). Seismic Profile A (MH44) in this study is situated above the relatively strongly coupled region of the plate interface at this location, where slip is thought to be accommodated co-seismically during large earthquakes (Clark et al., 2015; Wallace et al., 2009).

Table 1
Compiled Aspects of the Subduction Configuration Along the Hikurangi Margin

Margin section/ segment	North Hikurangi	Central Hikurangi	South Hikurangi – segment A (Profile A)	South Hikurangi – segment B (Profile B)	South Hikurangi – segment C (Profile C)
Latitude	38-40°S	40–41.25°S	41.5°S	42°S	42.5°S
Plate Motion Obliquity[a]	~30° (slightly oblique, at upper end of normal range)	50–60° (Moderately-highly oblique)	60° (Highly oblique)	85° (extremely oblique, margin parallel)	60° (Highly oblique)
Subduction velocity (mm/yr)[b]	45-60 (decreases southward)[1,2]	35-45 (decreases southward)[2]	~30[2]	~6.5[2]	~5.8[2]
Structure of incoming plate	Thin, distal turbidite sequence, atop rough basement studded with seamounts	Undeformed sequence of mostly fine-grained turbidites atop very smooth basement, but with some seamounts	Undeformed sequence of mostly fine-grained turbidites atop very smooth basement	Basement characterized by top of the west flank of the Chatham Rise accretionary complex and ancient Gondwana subduction trench fill. Pervasive normal (polygonal?) faulting through Chatham Rise cover, overlain by turbidites and coarser Hikurangi channel fill and levées	Basement characterized by top of the west flank of the Chatham Rise accretionary complex. Pervasive normal (polygonal?) faulting through Chatham Rise cover
Trench sediment thickness (km)[c]	<1.5[3]	3[4]	5 (3.5 TS + 1.5 HPCS)	9 (5.5 TS + 3.5 HPCS)	At C1 to T Bst: 3 (1.7 TS + 1.3 HPCS) At C1 to R8: ~9 (1.7 TS + ~7 HPCSS) At C4 (to R8): >9 (5.5 TS + ~4 HPCS)
Interseismic Coupling[5]	Weak	N-S transition from weak to strong	Strong	Weak	Weak
Stratigraphic position of the décollement at the deformation front	Variable - Seamount-controlled[6]	Condensed sequence of chalk and shale (Reflector 7)[7,8]	Condensed sequence of chalk and shale (Reflector 7)	Condensed sequence of chalk and shale (Reflector 7)	At C1 – unclear At C4 – Reflector 7
Presence of a prominent proto-thrust zone?	No[3,7,9]	Yes[9]	Yes	No	No
Taper[d]	>10° (α = >3°, β = >8°)[3]	<4° (α = 1–2°, β = 2–3.5°)[8]	~5° (α = ~2.2°, β = 3°)	~8° (α = ~3°, β = 5°)	>10° (α = ~3.3°, β = 7°)
Prism Width (km)	60[3]	130–150[7]	66	38	52
Fault Spacing (major thrusts) (km)	3-10 (some up to 15)[3]	3–10[8]	3–7	1–5	5–7
Thrust dip	25–60°[6]	30–45°[8]	30–45°	55–60° (<15 km landward of DF) 30–45° (>15 km landward of DF)	65° (<20 km landward of DF) 35–60° ramp-up geometry (>20 km landward of DF)
Estimated crustal shortening[e]	N/A	12%–16%[8]	21%	18%	3.5%
Structural distribution of shortening since 2 Ma	N/A	Uninhibited outward growth of the prism through propagation of new thrusts splaying from the décollement along reflector	Out of sequence slip on faults within the prism interior from 2 to 1 Ma, followed by predominantly in-sequence propagation of	Rapid in-sequence seaward propagation of new faults at the prism toe from 2 to 1 Ma, followed by period of minimal prism growth and	Propagation of major thrusts and backthrusts in sequence before 1 Ma, followed by a seaward jump of the

Table 1
Continued

Margin section/ segment	North Hikurangi	Central Hikurangi	South Hikurangi – segment A (Profile A)	South Hikurangi – segment B (Profile B)	South Hikurangi – segment C (Profile C)
		R7, but with continued deformation of the prism interior via slip on thrusts active out-of-sequence[7,8]	new thrusts at the prism toe continuing to present	very slow (low slip rate) development of faults in the prism interior	deformation front to pre-existing incoming structures

Note. Superscripts refer to following sources: 1. Wallace et al. (2004); 2. Wallace et al. (2018); 3. Barker et al. (2009); 4. Lewis et al. (1998); 5. Wallace, Barnes, et al. (2012); 6. Bell et al. (2010); 7. Barnes et al. (2010); 8. Ghisetti et al. (2016); 9. Barnes et al. (2018). DF = Deformation Front; C1, C4 = prism faults; R = Reflector; T Bst = top of the Chatham Rise Torlesse Composite Terrain (TCT) Wedge; TS = Trench Wedge Siliciclastics (R0-R5B); HPCS = Hikurangi Plateau Cover Sequence (R5B-R8). [a]Angle of incidence between absolute plate motion in degrees from orthogonal convergence (e.g., McNeill & Henstock, 2014) and does not account for strain partitioning (e.g., due to strike-slip activity). [b]Orthogonal convergence vector (mm/yr). [c]At present day deformation front. [d]Within 40 km of the deformation front for Segments A-C. [e]Reconstructed accommodated by major thrust-related deformation.

The strongly coupled interface of the southern Hikurangi margin has not experienced a major earthquake during the short (∼200 years) historic record (Clark et al., 2011), and the risk of a future earthquake and resultant tsunami remains highly uncertain (Wallace et al., 2014). However, recent palaeoseismic investigations have revealed evidence for at least four subduction earthquake events in the last 2000 years (Clark et al., 2015; Pizer et al., 2021), with the most recent event having occurred ∼500 years ago. Based on a recurrence interval of 500 years Pizer et al. (2021) determine a 26% probability of a >8.5 M_W earthquake occurring on the southern Hikurangi margin within the next 50 years.

Watson et al. (2020) compiled the changes in key subduction variables described above and, building on work by Lewis and Pettinga (1993), Collot et al. (1996), Barker et al. (2009), Pedley et al. (2010), Barnes et al. (2010), and Fagereng and Toy (2011), present the Hikurangi margin as broadly divided into three tectonic domains: (a) primarily seamount subduction and frontal tectonic erosion north of ∼40°S; (b) subduction accretion and low taper angle between ∼40°S and 41.5°S; and (c) subduction accretion and transpression south of ∼41.5°S. In this study we focus specifically on the region south of 41°S, and therefore within the 'subduction accretion and transpression' tectonic domain. We present the rationale for further sub-division of this southern-most tectonic domain of the Hikurangi margin.

The seismic data we present in this paper are widely spaced (∼100–200 km) but are representative of different subduction configurations, specifically the margin-normal subduction velocity, plate motion obliquity, and/or the morphology of the incoming Pacific Plate. The most notable morphological change along-strike is the increasing proximity and ultimate impingement of the southern Hikurangi margin on the continental Chatham Rise at to the south-west. The core of the Chatham Rise comprises the buried, Mesozoic accretionary prism referred to here as the Chatham Rise 'Torlesse Composite Terrane wedge' or Chatham Rise TCT wedge (e.g., Bland et al., 2015; Lee et al., 2002), which are equivalent strata to the 'Torlesse Composite Terrane' off Wairarapa (Figure 1; Bassett et al., 2022). Our study profiles also span significant along-strike changes in slip rate deficit on the subduction interface, reported by Wallace, Barnes, et al. (2012). Profile A is located within a zone of high slip rate deficit and strong interseismic coupling on the subduction interface (Figure 1b). Profile C crosses a region of low slip rate deficit (Figure 1b), due to the fact that relative plate motion is being transferred from the subduction interface to the upper plate dextral strike-slip faults of the Marlborough Fault Zone (Wallace, Barnes, et al., 2012). The subduction interface in this region can still accommodate some amount of slip, as demonstrated by the distribution of afterslip following the 2016 Kaikōura earthquake (Furlong & Herman, 2017; Mouslopoulou et al., 2019; Wallace et al., 2018; Wang et al., 2018).

Given the significant along-strike changes that occur from Profile A to Profile C (Figure 1b), over a distance of ∼220 km, we can use the profiles to make key inferences about the effect of different factors on forearc structure.

3. Methods

3.1. Data

We present three multichannel seismic reflection (MCS) profiles from the central-southern Hikurangi margin. One of the profiles is from the Seismogenesis at Hikurangi Integrated Research Experiment (SHIRE) project,

collected in 2017 by the R/V *Marcus G. Langseth* (Bangs et al., 2018a, 2018b; Gase et al., 2022). The *Langseth* acquired a total of 27 MCS profiles at the Hikurangi subduction zone from the Raukumara Peninsula to southern Wairarapa. Here we present profile MH44 (herein referred to as Profile A), for which we performed prestack-time migration. The SHIRE MCS data were acquired using a tuned 36 airgun array with 6,600 in^3 total volume. Shot spacing was 50 m, with recording on a 12.8 km long, 1,008 channel hydrophone streamer, towed at a depth of 8 m, and a recording time of 14 s at a 2 ms sample interval. Processing steps for profile MH44 included: resampling at 4 ms; trace balancing; bandpass frequency filtering (3–60 Hz); velocity analysis; suppression of seafloor multiples using surface-related multiple elimination (SRME) and radon filtering; and Kirchhoff prestack time migration. The other two MCS profiles, PEG09-17 (Profile B) and PEG09-09 (Profile C) are prestack-time-migrated data collected by the R/V *Reflect Resolution* during the New Zealand Government-funded PEG09 survey between November 2009 and March 2010 (Bland et al., 2015; PEG09, 2009; RPS Energy, 2010). Acquisition and processing details for the PEG09 data are summarized in RPS Energy (2010).

We complement the MCS profiles with a 25 × 25 m resolution bathymetry grid (MACKAY, 2023) and spatial positions of faults at the surface mapped by Mountjoy et al. (2009); Barnes et al. (2010); Wallace, Barnes, et al. (2012); Micallef et al. (2014); Ghisetti et al. (2016); and Crutchley et al., 2020).

3.2. Stratigraphic Interpretation and Depth Conversion

A number of studies have identified regional seismic reflectors within the incoming sediments of the Hikurangi Trough (Barnes et al., 2010; Ghisetti et al., 2016; Kroeger et al., 2022; Plaza-Faverola et al., 2012). These studies correlated the Hikurangi Plateau and cover sequence seismic units (including HKB, MES and Sequence Y) of Cretaceous and Paleogene age identified further east (Davy et al., 2008) to the Hikurangi Trough, and dated Neogene and Quaternary reflections through seismic ties to dated samples from the Chatham Rise and Hikurangi forearc slope. We interpret our seismic profiles according to the descriptions of the seismic character and intervals identified in these studies (Figure 2). In particular, we follow the nomenclature for seismic reflector marker horizons used by Barnes et al. (2010) and Ghisetti et al. (2016) to allow direct comparison and use seismic interval velocities between the markers derived by Ghisetti et al. (2016) for depth conversions of our profiles. We apply the age model defined by Ghisetti et al. (2016) for the inferred correlative reflectors (Figure 2). Our interpretation is most robust within the incoming sedimentary sequence, but with reasonable confidence the key horizons can be traced into the frontal accretionary prism. Transects of the seismic data were depth converted by applying interval velocities to seismic packages between the interpreted reflectors.

Reflector R7 marks the top of a sequence of widely traceable, high-amplitude reflections of relatively uniform thickness (0.1–0.2 s) which are identifiable in all three of our profiles. We interpret these reflections to constitute "sequence Y" of Wood and Davy (1994) and Davy et al. (2008), a condensed sequence of Late Cretaceous-Early Oligocene nannofossil chalks with alternating mudstones associated with the Hikurangi Plateau. Reflector R5B marks a regional unconformity which is primarily an onlap surface, but is locally erosional, associated with the western tilting of the Hikurangi Plateau (Barnes et al., 2018; Barnes & Mercier De Lépinay, 1997; Ghisetti et al., 2016; Lewis et al., 1998; Lewis & Pettinga, 1993; Pedley et al., 2010; Plaza-Faverola et al., 2012). It separates the siliciclastic trench wedge from the underlying Hikurangi Plateau sequence. Between R7 and R5B, reflector R6 marks the boundary between a weakly reflective interval that overlies R7 and a sequence of stronger reflections underlying R5B. Barnes et al. (2010) inferred the unit R5B-R6 to consist of nannofossil chalks interbedded with tephra and clay.

Onlapping onto the R5B regional unconformity is a clastic sequence of trench turbidites, within which the reflectors R5, R4, and R3 can be identified as markers separating units of different acoustic reflectivity (Barnes & Mercier De Lépinay, 1997; Barnes et al., 2010). Reflector R0 marks the seafloor. This sequence (R0-R5B) reaches a maximum thickness of ~6 km within the trench in our study area (Plaza-Faverola et al., 2012).

3.3. Progressive Retro-Deformation

To define the sequence of internal deformation within the accretionary prism and estimate the propagation/advancement rate of the southern Hikurangi accretionary prism deformation front and approximate crustal shortening, we performed retro-deformation analysis on the geological interpretation of each depth-converted transect of our seismic data using the MOVE software package (Midland Valley, 2014). Sections were restored by removing separation and folding across faults in order of activity from youngest to oldest and
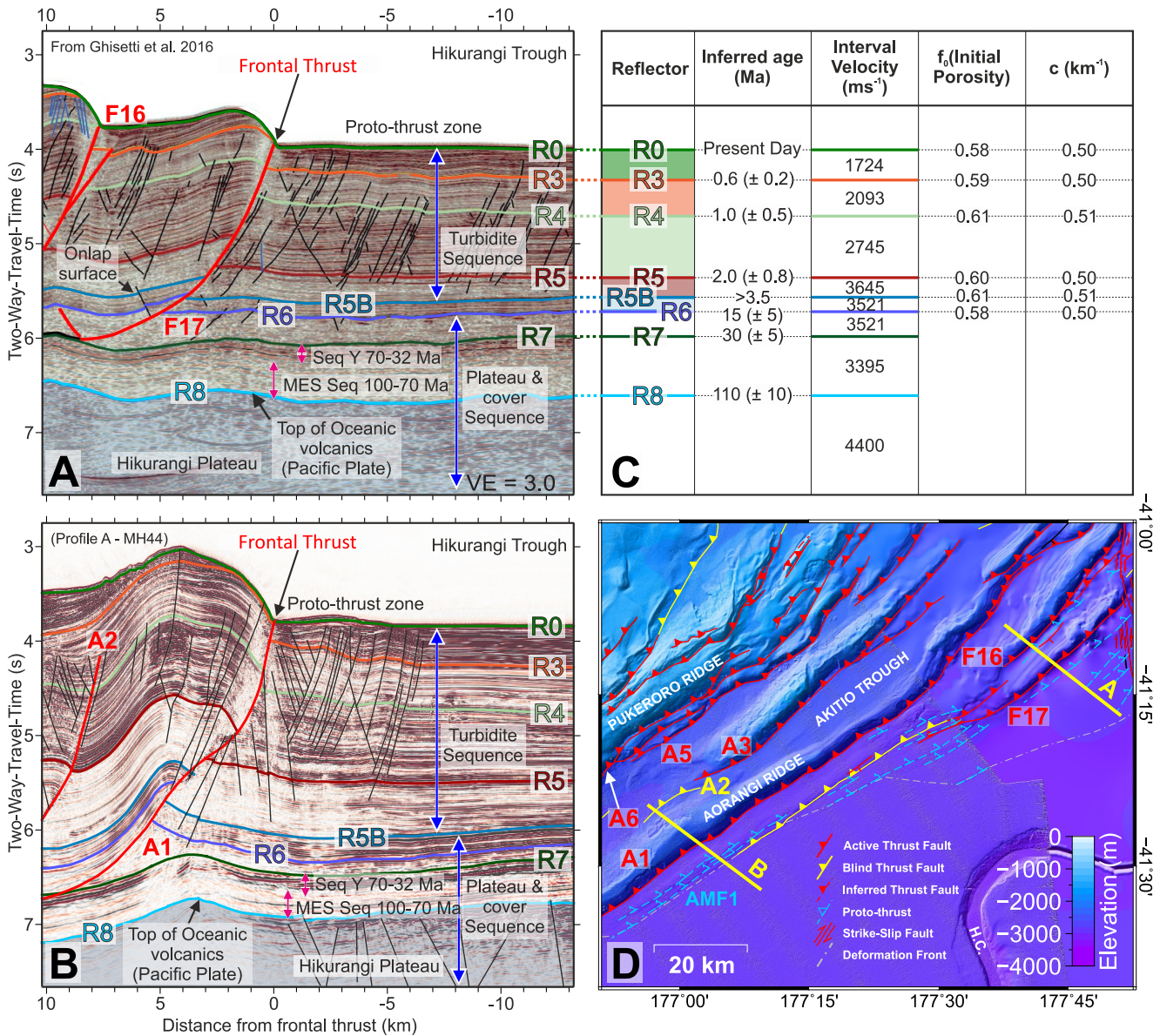
Figure 2. Stratigraphic interpretation and velocity structure. (a) Seismic data across the deformation front from Ghisetti et al. (2016) (location indicated in D) showing interpretation of major seismic marker horizons. Faults F16 and F17 refer to faults presented in Ghisetti et al. (2016). (b) Seismic data (part of seismic Profile A (MH44), location indicated in (d)) across the deformation front in our study area, showing interpretation of equivalent seismic marker horizons. For A and B, red lines are major thrust faults, thin black lines are minor faults (including proto-thrusts), sub-horizontal colored lines are marker horizons R0-R8. (c) Age, velocity, and physical property information for the sedimentary units between marker horizons, from Ghisetti et al. (2016): The parameter 'c' is the rate of change of porosity with respect to depth. (d) Bathymetry data showing locations of the two seismic sections shown in (a) and (b), as well as along-strike continuity of thrust faults F17 & F16 and A1 & A2.

incorporating progressive decompaction and back-stripping of restored sequences (See Text S1 in Supporting Information S1 for further detail).

It is important to note that the results of retro-deformation are non-unique due to a number of compounding factors. The structural geometry interpreted from the seismic data has inherent uncertainties that arise from uncertainties in tying to a regional framework of horizons, correlation across faults, and uncertainty in the velocities used for depth conversion. The profiles are approximately perpendicular to the strike of bathymetric ridges, so we suggest apparent horizon and fault geometries in the seismic data are close to their true geometry and that associated uncertainties are minimal. There are also choices in the precise methods of retro-deformation, and many deformation pathways achieve similar results. We limit the region for which we apply retro-deformation

restorations to 35–50 km landward of the subduction zone deformation front where stratigraphic horizons are better resolved and we have more confidence in horizon correlations across major thrust faults.

Most major faults imaged by our profiles have associated fault-propagation folds, with growth strata converging and/or onlapping onto hanging-wall anticlinal ridges. Following Ghisetti et al. (2016), we determine fault activity based on fault-controlled growth stratigraphy during each depositional interval (R0-R3, R3-R4, R4-R5, R5-R5B —from youngest to oldest) (See Figure S1 in Supporting Information S1). We hereafter refer to each depositional interval as a unit—for example, Unit R3-R4, meaning the unit between the top reflector (R3) and the basal reflector (R4). Due to reduced confidence in our seismic interpretation of the accretionary prism at depth we do not attempt detailed restoration prior to the deposition of the R5-R5B unit.

Following the restoration workflow outlined by Ghisetti et al. (2016) we restore fault-propagation folds by applying MOVE's trishear algorithm. Fault-propagation-folds generated by trishear kinematics are characterized by rounded anticlinal hinges and upward-shallowing dips in the footwall syncline. These folds are associated with faults that have concave geometries and ramp up-section but do not show staircase trajectories (typical of ramp-flat folds) (Tavani et al., 2005), with a linear up-dip decrease in fault displacement/horizon separation (All-mendinger, 1998; Erslev, 1991; Hughes & Shaw, 2014, 2015). Where there is no evidence of fault—propagation-folding associated with a fault, the displacement is removed by oblique simple-shear or fault-parallel shear kinematic models (Gibbs, 1983). Structures are restored in the order of their inferred activity history. After removal of all fault separation and folding, the fault is removed. Following repeated backstripping, the section was decompacted. See Texts S2 to S4 in Supporting Information S1 for the full breakdown of parameters used for fault restoration on each profile.

4. Results

Figure 3 shows the suggested subdivision of the southern Hikurangi margin into three structurally distinct segments (A, B, and C).

The key results within this paper are underpinned primarily by our interpretation of the three seismic reflection Profiles A-C where we have greatest confidence in our seismic interpretation of the outer margin. Interpretations of faults deeper and further landward in the prism become subjective where the seismic imaging does not resolve faults well. The poorer imaging further inboard and at greater depths is likely to be largely due to increased deformation in these parts of the prism. Note also that the extent of the Chatham Rise TCT wedge (position of the edge of the buried, ancient accretionary complex) has been mapped using existing legacy seismic data and is part of ongoing work to be published elsewhere. We acknowledge that the absolute value of shortening estimated from restored transects could be considered arbitrary, due to different profile lengths for each segment. Comparison of these shortening estimates between segments should be considered in the context of this caveat. However, the purpose of these estimates is to demonstrate the shortening that has been accommodated by the major, resolvable, outermost prism thrusts since 2 Ma. We consider the advancement rate of the frontal thrust (i.e., widening of the prism) to be a more useful metric for intersegment comparison.

4.1. Segment A

4.1.1. Structure of Segment A

4.1.1.1. Incoming Plate

The Hikurangi Trough in Segment A is underlain by an undeformed sequence of smooth, laterally continuous, sub-horizontal reflectors imaged by Profile A (Figures 3 and 4) atop a smooth layer of volcanics/volcaniclastics of the Hikurangi Plateau (Figure 4). Due to the proximity of the Hikurangi Channel, these reflections from ~3.8 to 6 s two-way-travel-time (TWT) (R0-R5B) largely represent relatively fine-grained turbidite sequences (McArthur & Tek, 2021; Tek et al., 2021). Profile A does not show significant evidence of buried channels within the trench (landward of the Hikurangi Channel). Total sediment thickness (from seabed to R8) within the trench is ~5 km at the deformation front (Figure 1). At this location the trench wedge is ~3.5 km thick and the underlying Hikurangi Plateau cover (below R5B) is 1.5 km thick.
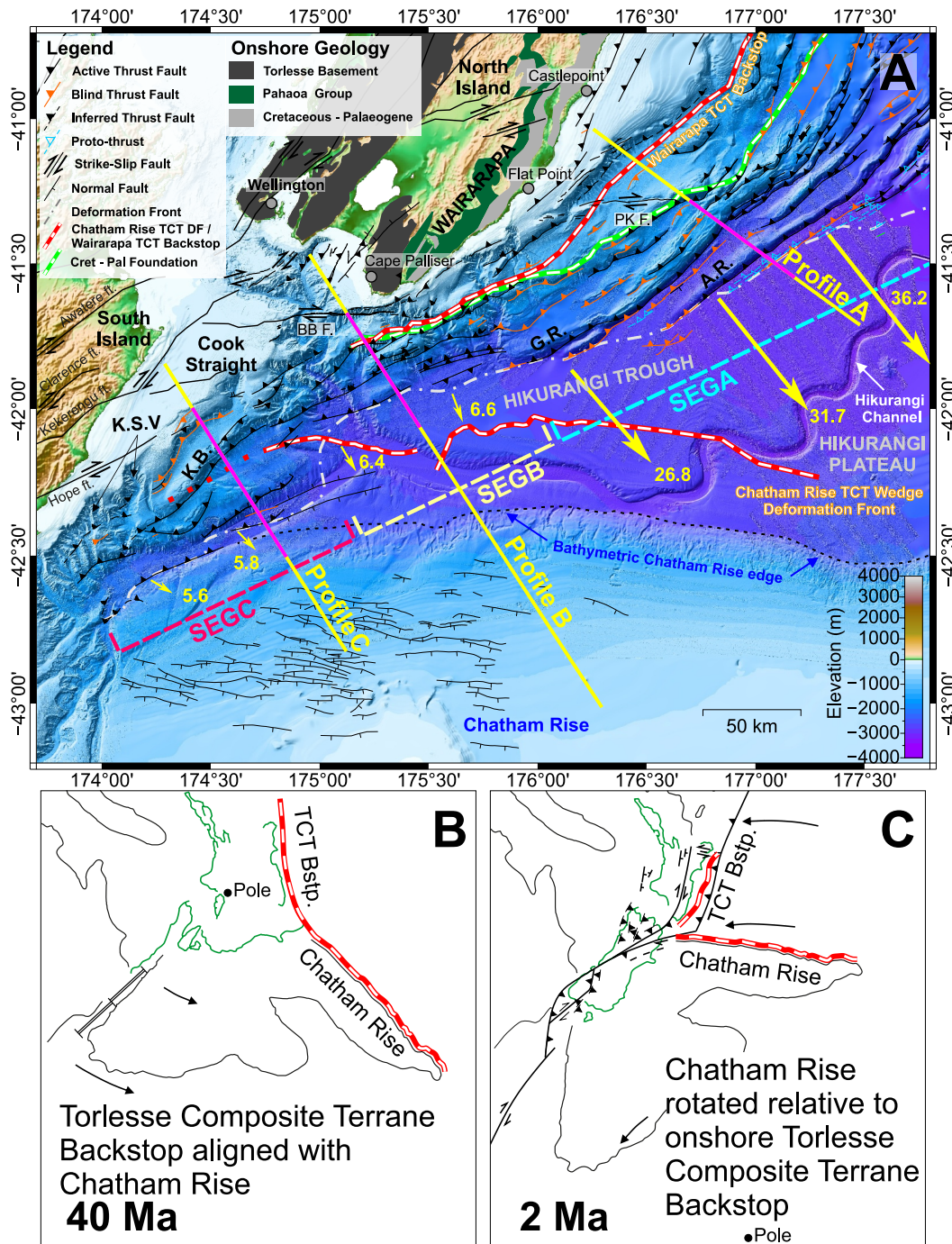
Figure 3. (a) Structure and segmentation of the southern Hikurangi margin. High-resolution (25 × 25 m) bathymetry data from our study area. Faults mapped are compiled from Mountjoy et al. (2009), Barnes et al. (2010), Wallace, Barnes, et al. (2012), Micallef et al. (2014), Ghisetti et al. (2016), and Crutchley et al. (2020). The position of seismic profiles and reconstruction transects are shown by yellow and magenta lines, respectively. Yellow arrows show the margin-normal subduction velocity at the Hikurangi trench (mm/year) (Wallace et al., 2018). Parts (b) and (c) show schematic reconstructions of the evolution of the Australian-Pacific plate boundary through the New Zealand subcontinent (King, 2000): Black arrows show vectors of Pacific plate rotation about an instantaneous pole (labeled black dot); red and white dashed line marks the extent of the inferred Torlesse Composite Terrane (which is split into the Wairarapa Backstop and Chatham Rise TCT wedge components in part A) at the two timesteps (Barnes et al., 2010; Bassett et al., 2022; Gase et al., 2021). SEGA, SEGB and SEGC refer to the structural segments described in the text. A.R. = Aorangi Ridge; G.R. = Glendhu Ridge; K.B. = Kekerengu Bank; K.S.V. = Kowhai Sea Valleys.
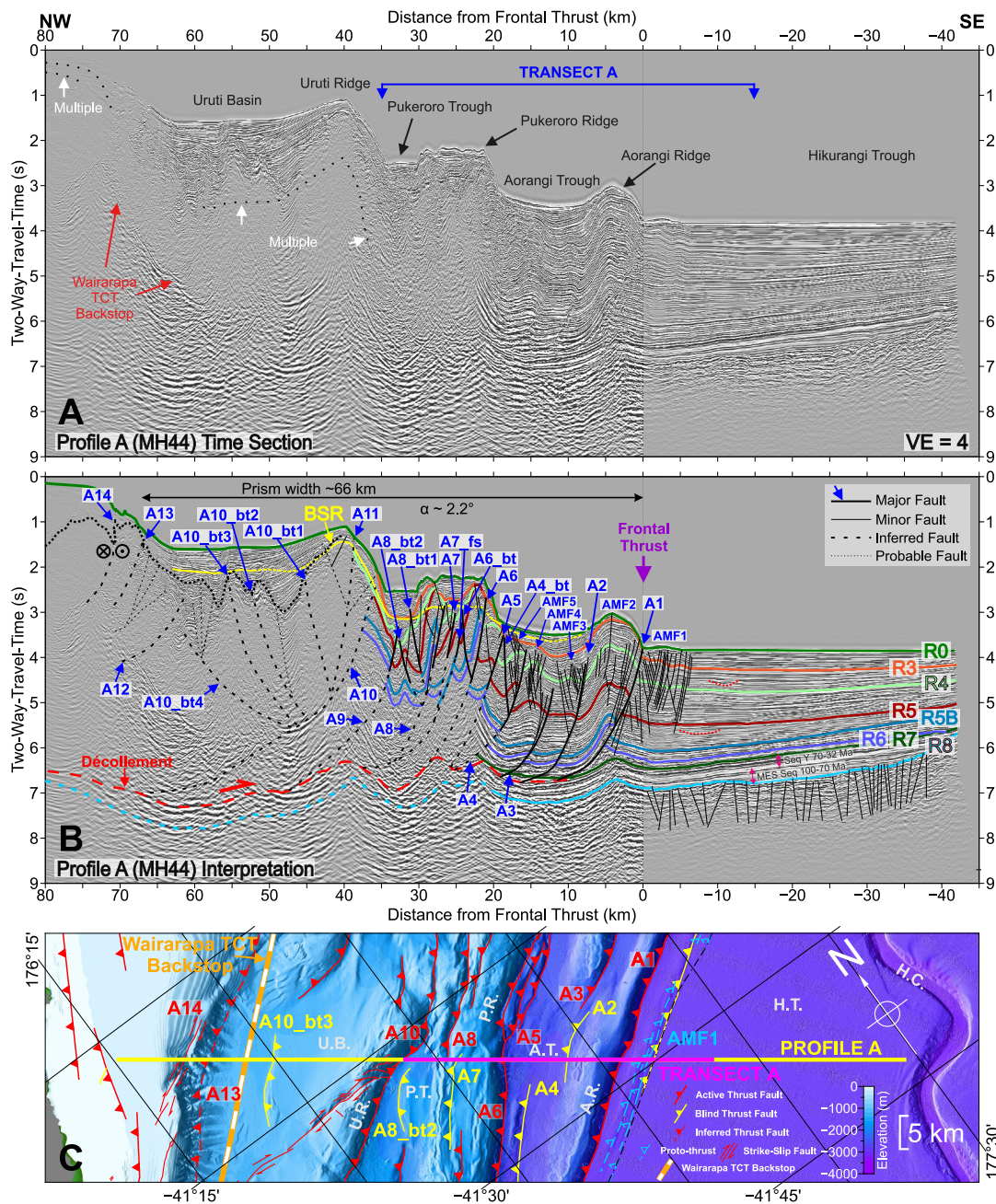
Figure 4. Seismic Profile A (MH44). (a) Pre-stack-time-migrated data without stratigraphic and structural interpretation, showing the positions of major bathymetric features and the extent of the depth-converted transect presented in Figure 5, for which we performed retro-deformation restoration (i.e., Transect (a)). Vertical exaggeration ("VE") for this and subsequent seismic sections displayed in TWT is based on water velocity (1,500 m/s). Note that gain has been increased landward of the deformation front to enhance visibility of features beneath the prism. See Figure S2 in Supporting Information S1 for the data displayed with reduced vertical exaggeration. (b) Stratigraphic and structural interpretation of the seismic data. Fault numbers correspond to those in (c) and Figure 5. Seismic marker horizons (R0-R8) are labeled. BSR = Bottom Simulating Reflection. Note wavy topography of the décollement is due to the data being displayed in Two-Way-Travel-Time (not depth). (c) Bathymetry (25 × 25 m) in the vicinity of Profile A showing faults mapped by Barnes et al. (2010) and Seebeck et al. (2023). Yellow line indicates seismic data displayed in (a) and (b), magenta highlight indicates restored section in Figure 5. A.R. = Aorangi Ridge; A.T. = Aorangi Trough; P.R. = Pukeroro Ridge; P.T. = Pukeroro Trough; U.R. = Uruti Ridge; U.B. = Uruti Basin.

4.1.1.2. Prism

The morphology and structure imaged by Profile A (Figure 4) is typical of other accretionary margins. Normal to the margin the prism is ~66 km wide from the deformation front to the updip extent of the Wairarapa TCT backstop mapped by Bassett et al. (2022) (Figure 3), with a surface slope (α) of ~2.2°. We approximate the basal slope angle (β, average dip of the décollement) from the depth-converted part of Profile A to be ~3°, giving a prism taper angle of ~5°. The frontal prism (within 40 km of the deformation front) consists of seaward-vergent thrusts, forming hanging-wall anticlines. Thrust dips are 30–45°, ramping up from shallower angles near their detachment points. Close to the shallowest expressions of major large-offset thrusts (e.g., A6 and A8), fault dips reach ~60°. Major thrusts have formed more prominent anticlinal ridges, with intervening piggy-back basins filled with growth strata. Major faults are spaced, on average, ~3 km, but spacing increases to as much as 7 km for the four outermost major thrusts (A1-A4).

There is a prominent ~7 km wide proto-thrust zone (AMF1, Figure 4) ahead of the frontal thrust, which can also be identified in the bathymetry. This proto-thrust zone continues to the northeast ahead of the frontal thrusts, where it is a common feature of a 200 km along-strike stretch of the margin (Barnes et al., 2010), but dies out ~35 km southwest of Profile A (Figure 3; Barnes et al., 2018). We observe minor faulting, similar in style to the proto-thrust zone, in the hanging-wall anticlines of the outermost frontal thrusts (A1-A4). These (AMF2-AMF5) may be ancient, accreted proto-thrust zones.

The décollement forms at the level of reflector R7 between the deformation front and fault A4. Despite poor seismic migration and velocity pull-up artifacts, it is inferred to be located on this horizon landward to at least Fault A10. The R7-R8 sediment sequence (Sequence 'Y' and the MES sequence) is therefore being subducted (Gase et al., 2022).

The outermost major thrusts appear to have formed in sequence, but there is evidence of continued activity on faults within the older part of the prism. Specifically, faults A8 and A6, which control the bathymetric expression of Pukeroro Ridge (Figure 4c) show significantly greater slip than faults further seaward and there is major thinning of the youngest sediment units at their hanging-wall anticline crests (Figure 4b). There is evidence of back-thrusting in the frontal prism, but it is minor and has very little impact on the prism morphology or accommodation of shortening (see later section). The more mature part of the prism (>40 km west from the deformation front) is poorly imaged due to multiple energy and the deformed nature of the sediments, and we were unable to confidently correlate seismic marker horizons R0-R7 landward of fault A10. However, we do identify several major faults within this part of the prism. Landward-vergent folding of seismic reflectors underlying Uruti Basin are interpreted as fault-propagation folds above back-thrusts that may detach into a major seaward-vergent fault beneath Uruti Ridge (either A10 or another unidentified fault between A10 and A12). Spacing of the controlling, seaward-vergent thrusts in this part of the prism is much larger (10–20 km) compared to the frontal prism (3–7 km).

Thrusts with the largest slip have prominent bathymetric expression and the greatest along-strike continuity (~70–145 km for faults A1 (Aorangi Ridge), A6 (Pukeroro Ridge), A8, A10 (Figure 4),). Although thrusts through most of the outer prism are spaced 3–7 km, prominent ridges created by those with the largest slip are spaced ~15–20 km in Segment A. The frontal thrust A1 has an ~145 km length, where to the northeast multiple younger thrusts have developed seaward of it. Back-thrusts in the deeper prism are shorter, for example, fault A10_bt3 has a length of ~20 km.

Seismic profile A appears to mark a divide, southwest of which strike-slip faults have been interpreted within the inner prism (Barnes et al., 1998, 2010; Seebeck et al., 2023). The Palliser-Kaiwhata strike-slip fault's eastern tip is located immediately southwest of the profile, where it appears to link to fault A10 (Uruti Ridge; Figure 3). Northeast of this profile, strike-slip faults are not observed within the prism interior (Ghisetti et al., 2016) but have been identified locally across the deformation front of the central margin (Barnes et al., 2018; Davidson et al., 2020) (Figure 3).

4.1.2. Structural Evolution of Segment A Prism From Restoration

Progressive retro-deformation restoration modeling allows for the quantification of the shortening accommodated by fault activity along a finite length of each seismic profile and the relative seaward advancement rate of the frontal thrust. By comparing the amount of estimated shortening to the advancement rate of the frontal thrust and

the variables between the seismic profiles, we can deduce possible mechanisms that account for the observed structural variation along the Hikurangi margin.

In the following section, and Sections 4.2.2 and 4.3.2, where advancement of the frontal thrust is quoted this refers to total seaward advancement of the frontal thrust toward a point fixed on the incoming plate. This includes both seaward fault propagation (i.e., formation of a new frontal thrust), and the effects of contraction of the prism facilitated by continued slip on faults in the prism interior. The latter results in advancement of the frontal thrust position relative to the fixed point even if there is no new fault formed. Note that advancement rates between stages are given as best estimates due to the overlapping age ranges for each stage.

Overall, based on Profile A the outer prism in Segment A experienced a period of high sedimentation rate relative to contraction during deposition of unit R4-R5, followed by more rapid seaward propagation of the décollement and growth of the prism.

Prior to the deposition of unit R5-R5B, the prism at Profile A was deformed by major thrusts A8 and A6 and associated back-thrusts, with fault A5 likely beginning to propagate from the décollement to form the deformation front (Stage 1, Figure 5a). These faults continued to be active through deposition of unit R4-R5, contemporaneously with the propagation of a new in-sequence seaward-vergent frontal thrust A4 (Stage 2, Figure 5b). This corresponds to an advancement of the frontal thrust between Stages 1 and two of ~6.7 km, at an approximate rate of 6.7 km/Myr.

During the deposition of unit R3-R4, there was significant fault activity throughout the prism landward of fault A4 including faults A7 and A7_fs propagating within the older prism, developing as splays from fault A8 (Figure 5c) or possibly from the décollement. However, there was no seaward propagation of the deformation front, which remained at fault A4. Large displacement occurred on faults A8 and A6, which developed prominent propagation folds and likely resulted in thinning of unit R3-R4 at their anticlinal crests and possible associated erosion of the uplifted unit R4-R5 (Stage 3, Figure 5c). The displacement on these and other faults within the prism interior resulted in substantial contraction of the prism and a relative seaward advancement of the frontal thrust by ~1.5 km relative to Stage 2, corresponding to an advancement rate of 3.75 km/Myr.

During deposition of unit R0-R3 (i.e., between Stages 3 and 4; Figures 5c and 5d), there was rapid seaward propagation of the décollement, with the frontal thrust advancing from fault A4 to A3, A2 and then A1, with minor fault zones developing either ahead of these faults, probably as proto-thrust zones, or within the anticlinal crests of the associated propagation folds. During this time there was continued activity at faults A4, A5, A6 and A8. Faults A3 and A2 likely ceased to be active prior to, or during the very early stages of the deposition of unit R0-R3 and folding associated with these faults is minor relative to fault A1, where the deformation front has been located since at least 0.1 Ma (Stage 4, Figure 5d). Total relative advancement of the frontal thrust between Stage 3 and 4 was ~18.8 km, equating to an approximate advancement rate of 37.5 km/Myr.

Continued propagation on fault A1 between Stage 4 and Stage 5 (Figure 5e), and continued activity of faults A5, A6 and A8, suggested by thinning of unit R0-R3, resulted in further shortening, and relative advancement of the frontal thrust by ~0.5 km, corresponding to an approximate advancement rate of 5 km/Myr. The bathymetric expression of the proto-thrust zone seaward of fault A1 (Figure 4b) indicates that the new frontal thrust is already beginning to form at the zone's seaward edge.

Excluding the proto-thrust zone, our restoration suggests a total overall relative advancement of the frontal thrust between Stage 1 and Stage 5 (since ~2 Ma) of 27.5 km. Accounting for errors in age, this corresponds to an advancement rate of between 9.8 and 22.9 km/Myr, and a best estimate of 13.75 km/Myr, which is somewhat slower than the 20–30 km/Myr rate estimated by Ghisetti et al. (2016) for the widest part of the Hikurangi prism for the same period.

The relative change in length of the restored section of Profile B at Stage 1 from 63.425 km (original length L_0) to 50 km (final length L_f) at the present day (Stage 5) requires a total estimated profile-parallel linear strain of ~21%.
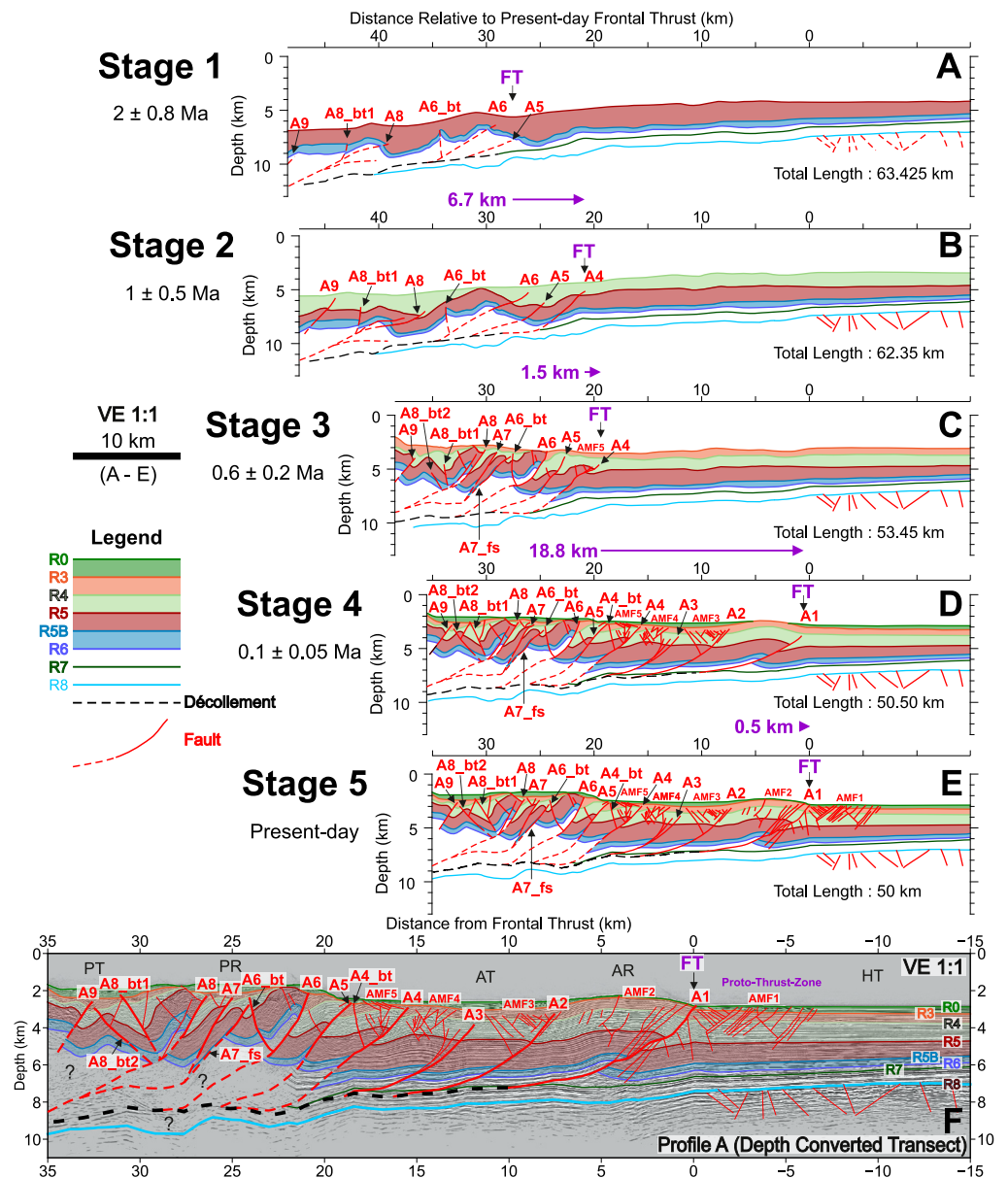
Figure 5. Retro-deformation restoration of depth converted transect of seismic Profile A. a-e) The evolution of the prism over the last 2 Myr, where each stage shows the pre-deformed state at the end of deposition of the youngest sediment unit at each time. f) Depth converted seismic data showing interpretation. Colored lines labeled R0 to R8 are seismic marker horizons. Red lines are faults; fault numbers correspond to Figure 4. See Text S2 in Supporting Information S1 for full breakdown of retro-deformation steps.

4.2. Segment B

4.2.1. Structure of Segment B

4.2.1.1. Incoming Plate

Seismic Profile B (PEG09-017, Figure 6) images a very different incoming plate geometry from Profile A (MH44). The subduction trench is relatively narrow, with the trench-wedge onlapping onto the northern flank of the Chatham Rise and Hikurangi Plateau, which dips ~6° to the north, toward the subduction zone (Figure 7f; Plaza-Faverola et al., 2012; Bland et al., 2015). The thickness of the trench-wedge sequence (R0-R5B) increases significantly from its pinch point ~55 km from the deformation front, where the top of the Chatham Rise cover
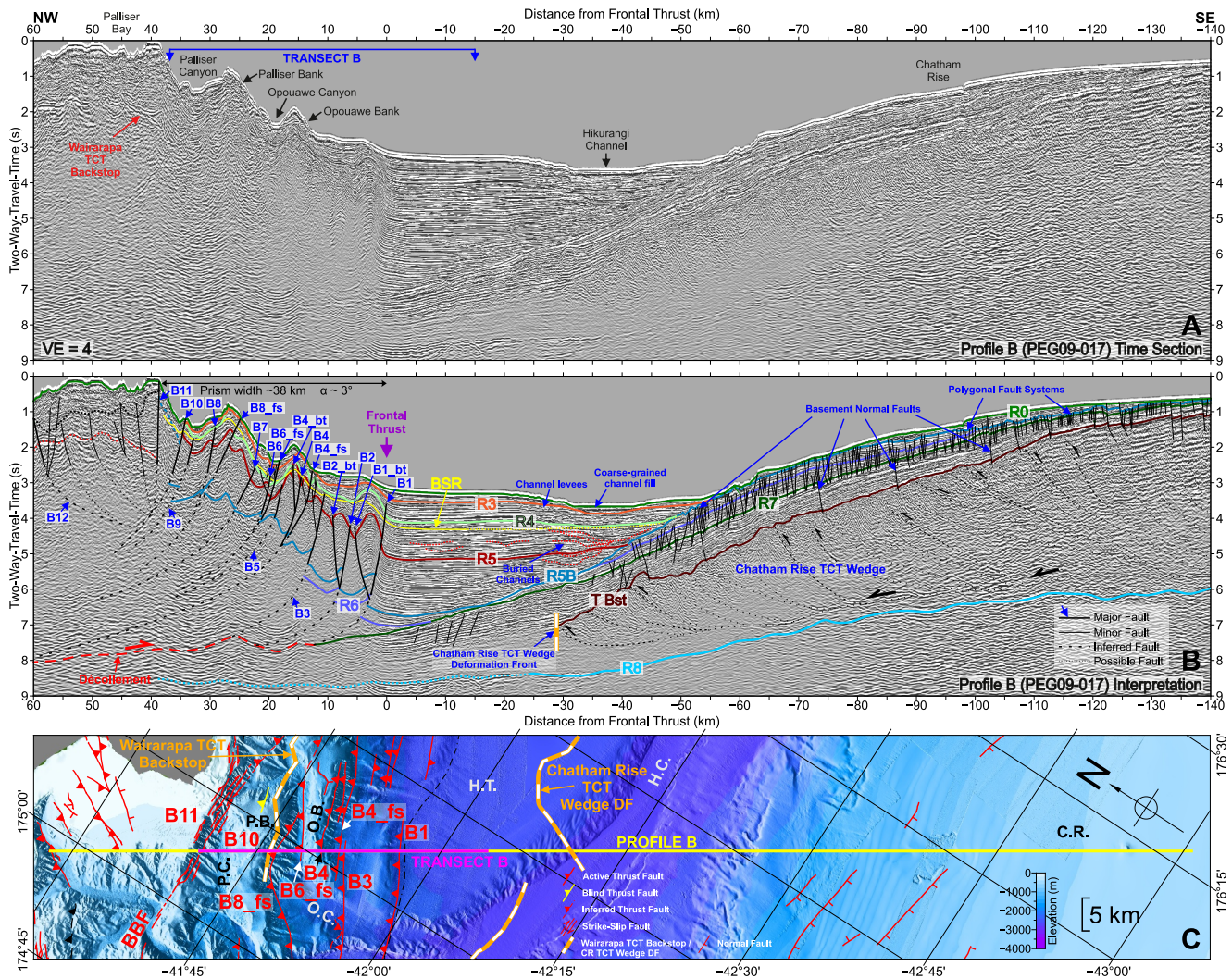
Figure 6. Seismic Profile B (PEG09-017). (a) Pre-stack-time-migrated data without stratigraphic and structural interpretation, showing the positions of major bathymetric features and the extents of the depth-converted transect (Figure 7) for which we performed retro-deformation restoration. See Figure S3 in Supporting Information S1 for the data displayed reduced vertical exaggeration. (b) Stratigraphic and structural interpretation of the seismic data. Fault numbers (in blue) correspond to those in (c) and Figure 7. Seismic marker horizons (R0-R8) labeled as in Figures 2B and 4. BSR = Bottom Simulating Reflector. (c) Bathymetry (25 × 25 m) in the vicinity of Profile B showing faults compiled from Mountjoy et al. (2009), Barnes et al. (2010), Wallace, Barnes, et al. (2012), Micallef et al. (2014), and Crutchley et al. (2020). Yellow line indicates seismic data displayed in (a) and (b), magenta highlight indicates restored section in Figure 7. Orange and white dashed line in the NW indicates the outer extent of the Torlesse Composite Terrane beneath the Wairarapa margin, whilst that beneath the Hikurangi Trough is the up-dip extent of the equivalent terrane beneath the northern Chatham Rise. O.B. = Opouawe Bank; O.C. = Opouawe Canyon; P.B. = Palliser Bank; P.C. = Palliser Canyon.

sequence (reflector R5B) outcrops at the seafloor, to ~5.5 km at the deformation front. When the underlying Hikurangi Plateau cover sequence (R5B-R8) is also included, total sediment thickness is ~9 km at the deformation front (Figure 7f; Plaza-Faverola et al., 2012). The top of the Hikurangi Plateau (R8) is imaged between 6.0 and 8.6 stwtt beneath the Chatham Rise, Hikurangi Trough, and frontal accretionary prism (Figure 6). The Hikurangi Channel is crossed by Profile B, with a well-developed channel levee sequence imaged on its northwest bank (Figure 6) (McArthur & Tek, 2021; Tek et al., 2021). The more chaotic seismic character within and below the channel and evidence of ancient, buried channels within the trench wedge (Figure 6) suggest that the incoming sediments through Segment B include channel facies and hence likely coarser-grained material relative to Segment A. We note that seafloor sediment samples from the present-day channel have recovered gravelly and sandy turbidites (Howarth et al., 2021; Lewis & Pantin, 2002; Mountjoy et al., 2018). The trench-wedge sediments appear to be otherwise undeformed. Conversely, normal faults are pervasive through the Chatham Rise cover sequence, where they terminate down-dip at or near reflector R7. Bland et al. (2015) interpreted many of these faults as
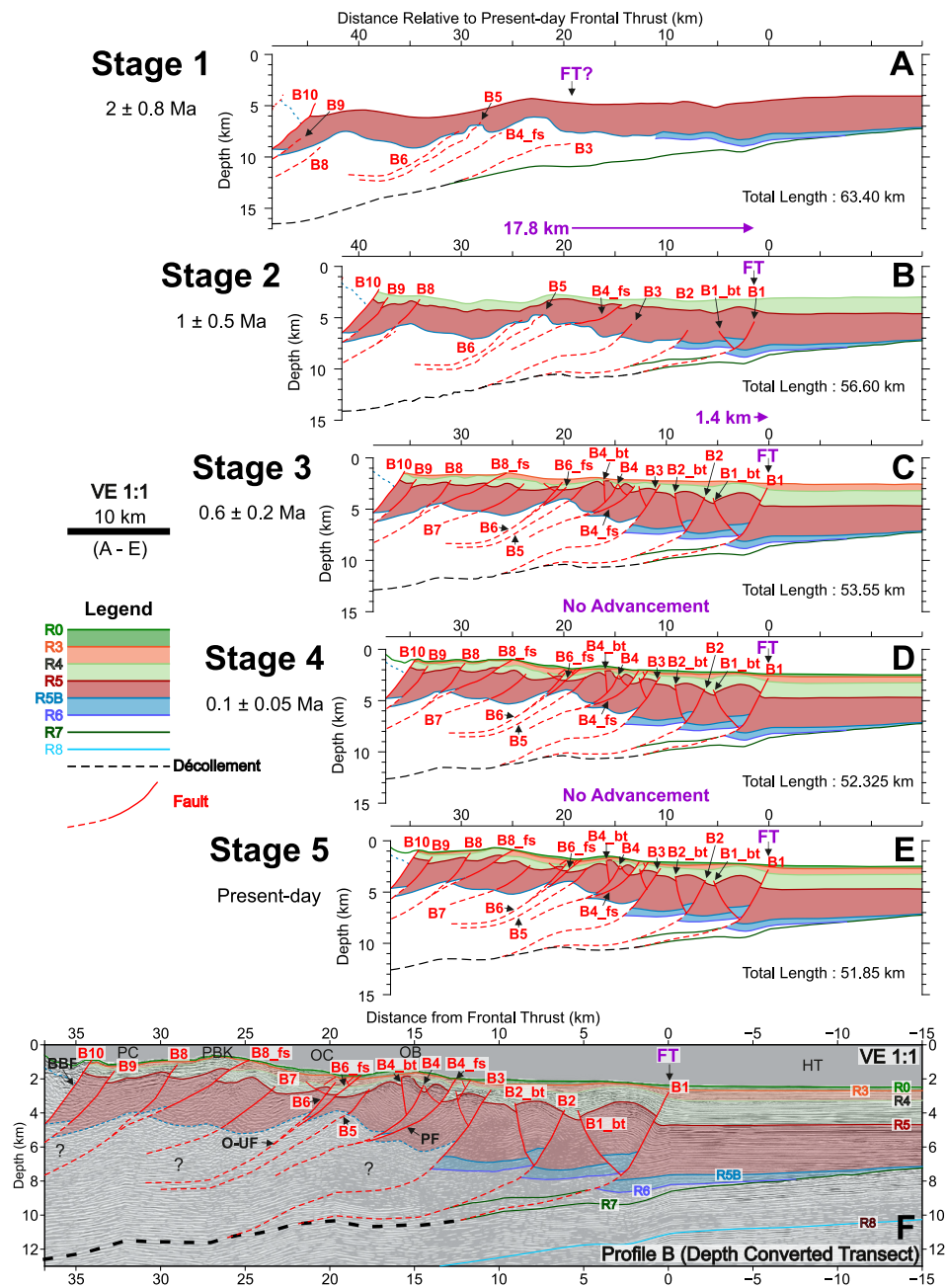
Figure 7. Retro-deformation restoration of depth converted transect of seismic profile (b). (a)-(e) The evolution of the prism over the last 2 Myr, where each stage shows the pre-deformed state at the end of deposition of the youngest sediment unit at each time. (f) Depth-converted seismic data showing interpretation. Sub-horizontal colored lines indicate seismic marker horizons. Fault numbers correspond to Figure 6. See Text S3 in Supporting Information S1 for full breakdown of retro-deformation steps.

polygonal faults forming in the fine-grained deep-water sediments. Underlying this cover sequence is the Mesozoic Gondwana subduction zone accretionary prism that resulted from subduction of the Hikurangi Plateau beneath the Chatham Rise (Davy et al., 2008)—the TCT wedge. On Profile B (Figure 6) the ancient deformation front of this now inactive imbricate thrust sequence is located ~30 km seaward of the modern day Hikurangi deformation front. These inactive thrust faults were seaward-vergent during Gondwana subduction and now dip away from the Hikurangi subduction zone. The top of the TCT wedge forms an undulating basement surface. Basement involved normal faults beneath the upper Chatham Rise slope are part of the North Mernoo Fault Zone (Barnes, 1994).

4.2.1.2. Prism

There is a gradual narrowing of the prism between segments A and B (Figure 3) in association with progressive landward stepping of the deformation front from north to south (e.g., Barnes & Mercier De Lépinay, 1997; Lewis & Pettinga, 1993). The prism width on Profile B is narrower than Profile A, whether the backstop to the prism is defined as the seaward extent of the Torlesse complex (~35 km) or to the Boo-Boo strike slip fault (~38 km), and the seafloor slope angle (α) is ~3°. Similar to Segment A, the prism is characterized by predominantly seaward-vergent thrusts, however, there is antithetic back-thrusting that results in pop-up anticlines in the outermost prism, also observed south of Aorangi Ridge (e.g., Kroeger et al., 2022; Turco et al., 2020). There is no proto-thrust zone on seismic Profile B. Hanging-wall anticlinal ridges are less well developed compared to Segment A, and the piggy-back basins imaged by Profile B are narrower, shallower and less filled than those on Profile A. The latter is likely partly due to erosion related to the Cook Straight canyon tributaries (Figure 3). Spacing of the major thrusts is 1–5 km (5 km between the outermost thrusts B1–B3, excluding back-thrusts). Thrust dip >15 km landward of the deformation front is 30–45°, but the outermost thrusts and their back-thrusts ramp up to 55–60° dip (Figure 7f). Sediment units between the seismic horizons R5 and R0 on Profile B are generally thinner compared to Profile A. However, the sequence provides evidence for continued thrust activity in the prism interior. Faults B4_fs and B8_fs show large amounts of displacement offsetting Reflector R5, relative to thrusts further seaward, suggesting that although they have formed prior to the propagation of thrusts B1–B3 (and B5–B7), there has been continued activity on them.

Similar to Profile A, we interpret the contemporary décollement to initiate at reflector R7 at the deformation front on Profile B. We approximate a basal slope angle (β), from the depth-converted transect B, of ~5°, giving a taper angle of ~8°.

Although most thrust faults on Profile B are blind (Figure 6), we can infer their along-strike continuity from the seafloor expression of hanging-wall anticlinal ridges (Figure 3) and match them to pre-existing fault maps. However, this is made more difficult by the presence of the Cook Strait canyon to the southwest of the seismic profile, and there are previous interpretations that differ from each other in this area (Crutchley et al., 2020; Micallef et al., 2014). Nevertheless, it is clear that faults in Segment B are shorter along-strike than faults in Segment A: generally, 20–40 km (Figure 3).

Faults B10 and B11 on Profile B constitute the dextral Boo-Boo strike-slip fault (Mountjoy et al., 2009), which appears to act as a back-stop to imbricate thrusts within the prism. Seismic imaging beneath the outer Palliser Bay is poor, however there are displaced and folded reflections indicating the presence of landward-vergent folds, which we interpret to be back-thrusts (or oblique back-thrusts) off fault B10 (the strike-slip Boo-Boo fault).

4.2.2. Structural Evolution of Segment B Prism From Restoration

Based on folding and uplift of R5B, it is possible that a number of major seaward-vergent thrusts within the Segment B prism had already propagated prior to the deposition of unit R5-R5B, with a blind deformation front at fault B3 (Stage 1, Figure 7a). Significant thinning of unit R5-R5B (Figure S1 in Supporting Information S1) suggests that there may have been significant basement relief associated with some of these early structures (e.g., B3, B5, Figure 7a).

Following the deposition of unit R5-R5B, multiple faults (e.g., B9, B8 and B4_fs) propagate up through the deeper part of the prism and there is seaward advancement of the deformation front as faults B3, B2, and B1 propagate through unit R5–R5B (Stage 2, Figure 7b). By this stage the frontal thrust is fault B1, the present-day frontal thrust, and the displacement on B1 exceeds that of B2 and B3 at Stage 2, indicating a slow-down of seaward fault propagation and the concentration of slip on this fault. Progressive removal of the displacement on faults, flattening of horizons, and back-stripping through the retro-deformation process suggests the sediment accumulation rate during deposition of unit R4–R5 (between Stage 1 and Stage 2) probably exceeded the rate of upward fault propagation for the outermost faults during the same period (most contemporary fault displacement is restored during the later stages, leaving only minor displacement to be restored to flatten the R4 horizon (Figure 7b, Stage 2; see Text S3 in Supporting Information S1).The total relative advancement of the frontal thrust between Stage 1 and 2 was ~17.8 km, therefore corresponding to an approximate advancement rate of 17.8 km/Myr.

During deposition of unit R3–R4 (between Stage 2 and Stage 3) there was continued activity and propagation of thrusts within the prism interior propagate, and several additional thrusts also formed within the prism interior out-of-sequence, specifically B8_fs, B7, B6_fs and B4. Back-thrusts B2_bt and B1_bt, and possibly B4_bt, also developed during this period. Activity on these faults resulted in only minimal relative advancement of the frontal thrust between Stage 2 and Stage 3 of 1.4 km, equating to an approximate advancement rate of 3.5 km/Myr. The resultant fault structure (Stage 3, Figure 7c) then remained relatively fixed throughout deposition of units R3-R4 and R0–R3 (up until Stage 5) with minimal fault displacement. Small amounts of displacement on faults B1, B4_fs and B8_fs, result in minor contraction of the prism, but no discernible relative advancement of the frontal thrust.

Overall, the total relative advancement of the frontal thrust between Stage 1 and Stage 5 was ∼19.2 km, and accounting for errors in age, this corresponds to an advancement rate of between ∼6.9 and 16 km/Myr, with a best estimate of 9.6 km/Myr. However, importantly, our results suggest that all of the advancement took place prior to 0.6 Ma, and mostly before 1 Ma.

The change in length of the restored section of Profile B from 63.40 km (original length L_0) at Stage 1–51.85 km (final length L_f) at the present-day (Stage 5) requires a total estimated profile-parallel linear strain of ∼18%, similar to Profile A but occurring mostly between 2 and 1 Ma for Profile B.

4.3. Segment C

4.3.1. Structure of Segment C

4.3.1.1. Incoming Plate

Seismic profile C (PEG09-009, Figure 8), images a similar structure to Profile/Segment B, but with added impact of the subducting ancient TCT wedge. In Segment C the Hikurangi margin is impinging on the TCT wedge, which is thus partially underthrusted. We infer the Chatham Rise TCT wedge deformation front to be at least 25 km landward of the contemporary Hikurangi deformation front at fault C1 (Figure 8). Consequently, the lower part of the MES sequence, which constitutes the ancient Gondwana subduction trench sedimentary sequence (and would have been subducting in an opposite direction to the present-day trench sediments, Figure 3) is not well-resolved on Profile C. The Chatham Rise TCT wedge is covered by upper Cretaceous to Recent sediments and underlain by oceanic Hikurangi Plateau volcaniclastics (R8). The entire trench wedge (horizons R5B to R0) here is essentially deformed with active structures extending out to be the Hikurangi Channel lying at the base of the Chatham Rise slope (Crutchley et al., 2020). However, for reference at fault C1, the sediment thickness is 3 km when the Chatham Rise TCT wedge is considered as basement, or ∼9 km when the Chatham Rise TCT wedge is included (Table 1). Fault C1 is only ∼12 km from the lower slope of the Chatham Rise, where the base of the trench wedge (Reflector R5B) lies close to the seafloor (Figures 3 and 8). Therefore, the TCT wedge and its cover sequence define the incoming Pacific plate structure in Segment C. Its characteristics are: an undulating basement surface formed at the top of the ancient prism; the now-inactive imbricate thrust sequence of the ancient prism, with faults dipping away from the modern subduction zone; and the Chatham Rise cover sequence. Similar to seismic Profile B we observe normal faulting through the cover sequence involving basement (Barnes, 1994).

4.3.1.2. Prism

The southern Hikurangi margin Wairarapa TCT backstop was not mapped as far south as Profile C by Bassett et al. (2022), but by projecting its extent to the south and considering the possible basement pick on Figure 4b, we suggest it underlies the eastern Marlborough shelf adjacent to where it is widely exposed onshore (Rattenbury et al., 2006) and likely extends close to our Fault C6 (Figure 8). Given this assumption, the prism width (between the shelf break and fault C1 is ∼52 km indicating an increase in prism width between profiles B and C (Figure 8). There is also a significant seaward outstepping in the position of the deformation front south of the Cook Strait Canyon into the Hikurangi Channel that is broadly coincident with the impingement of the Hikurangi margin on the TCT wedge (Figure 3). The prism slope is relatively steep at ∼3.3° and we approximate a basal slope angle (β) of ∼7° for the outer 40 km of the prism from the depth-converted transect C, giving a taper angle of >10° (Table 1). At Profile C there is virtually no trench wedge, as the deformation front has propagated out to the position of the north-dipping Chatham Rise flank. Regional seismic reflection data southwest of the profile (Crutchley et al., 2020) suggest that the deformation front steps to the east and further from the hinterland
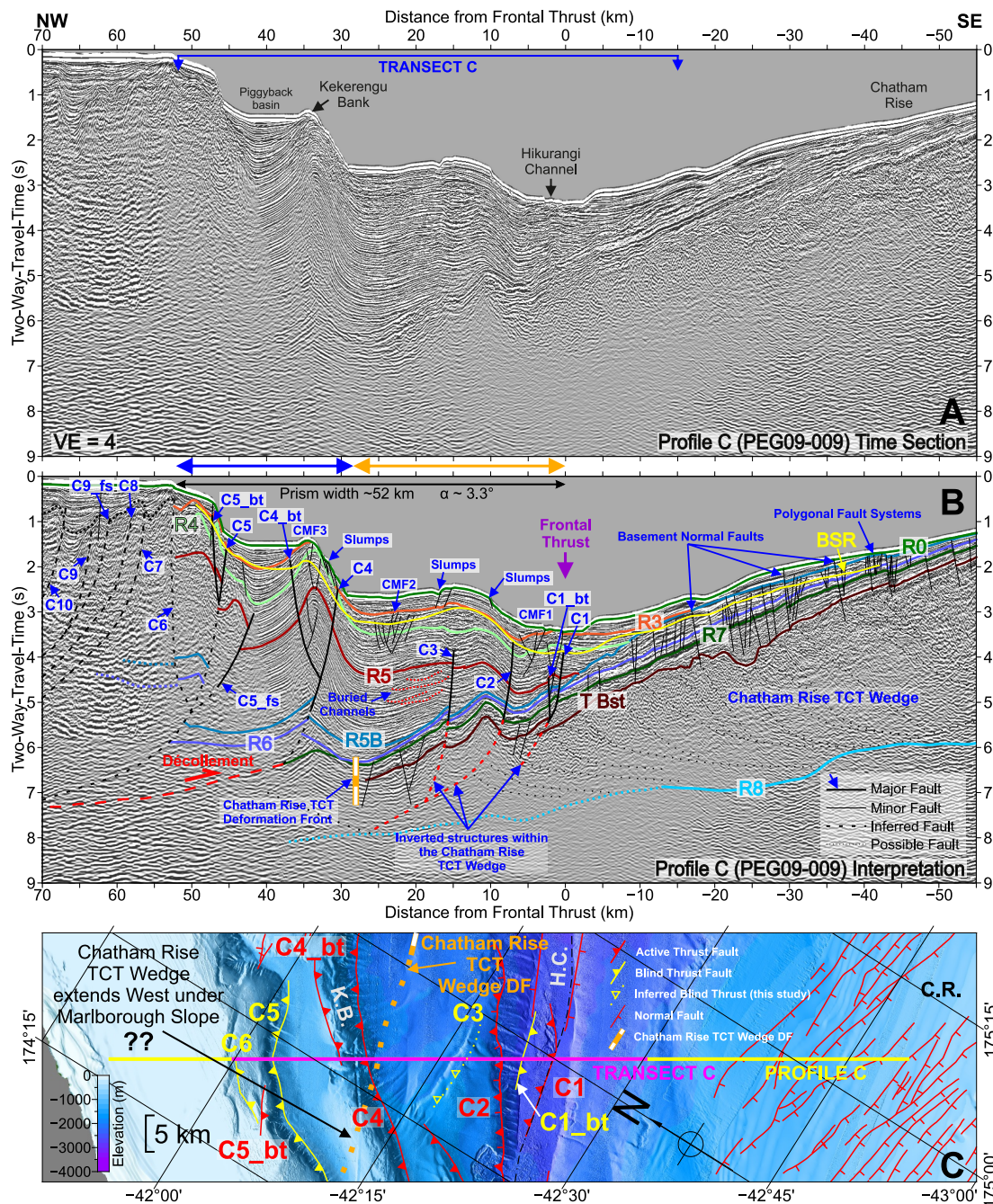
Figure 8. Seismic Profile C (PEG09-009). (a) Pre-stack-time-migrated data without stratigraphic and structural interpretation, showing the positions of major bathymetry topographic features (see Figure 3) and the extent of the depth-converted transect (Figure 9), for which we performed retro-deformation restoration. See Figure S4 in Supporting Information S1 for the data displayed reduced vertical exaggeration. (b) Stratigraphic and structural interpretation of the seismic data. Fault numbers correspond to those in (c) and Figure 9. Sub-horizontal colored lines are seismic marker horizons (R0-R8). BSR = Bottom Simulating Reflector. (c) Bathymetry (25 × 25 m) in the vicinity of Profile C showing faults modified from Wallace, Barnes, et al. (2012), Crutchley et al. (2020), and Barnes (1994). Yellow line indicates seismic data displayed in (a) and (b), magenta highlight indicates restored section in Figure 9. Orange and white dashed line indicates the extent of the Torlesse Composite Terrane. The blue arrow indicates extent of the prism unaffected by fault reactivation, and the orange arrow indicates the part of the prism which includes components of fault reactivation within the Chatham Rise TCT wedge.

(Figure 3). Faults are sparse, mainly seaward vergent, and spaced 5–7 km. The Hikurangi décollement on Profile C is difficult to define at the position of fault C1: Though we show offset of the top of the TCT wedge (T Bst, Figure 8), it is possible that there is strain partitioning at the reflector R7 level (see interpretations by Crutchley et al., 2020). Regardless of the precise position of the contemporary décollement, we interpret that the outermost

prism faults (C1-C3) are reactivated structures associated with the TCT wedge (Figure 8). Landward of Fault C4, we interpret the décollement forming at R7, consistent with Crutchley et al. (2020). The inner faults (landward and inclusive of C4) ramp up in dip from ~35° to ~60°, whereas the outer faults (C1–C3) are more planar with dip angles up to ~65°. There is a ~15 km across-prism gap where we interpret no major thrust faults between faults C3 and C4. These observations are atypical of the prism thrusts formed normally and in-sequence. Additionally, on Profile C we observe folding of the TCT bst horizon and entire cover sequence (Figures 8, ~10 km from the deformation front) by what appears to be deformation deeper within the Chatham Rise TCT wedge. Hence our interpretation that faults C1–C3 are reactivated structures corresponding to the positions of the older faults.

Young growth strata in the basin landward of Kekerengu Bank indicates continued activity on faults C4 and C5 to the present day, whilst faults further seaward have initiated/propagated. There is a major back-thrust (C4_bt) from fault C4, together responsible for the uplift of Kekerengu Bank, which shows evidence of recent slumping on its seaward flank (Figures 8 and 9). There are several minor fault zones (CMF1-4), however these differ from the characteristic prominent proto-thrust zone of Segment A. Pronounced downward bending of reflections exists between ~10 and 15 km landward of the deformation front, from approximately 3 s TWT downwards (Figure 8). This downward bending is a velocity artifact (a pull-down effect) caused by a thick, interconnected free gas column beneath gas hydrates (Crutchley et al., 2016, 2018) and therefore the precise nature of structural deformation in this upper part of the prism is unclear.

Along-strike, the typical length of the faults in Segment C is ~40 km (Figure 3). The north-eastern tips of these faults terminate southwest of the Cook Straight Canyon and the Segment B faults. Apart from Kekerengu Bank (Figure 3), hanging-wall anticlinal ridges are not as prominent in Segment C as Segment A, and are somewhat obscured by erosion related to the Kowhai Sea Valleys, south of Kekerengu Bank (Figure 3). The dip-slip offset on the outer thrusts within the prism (C1-C4) is relatively small, on the order of 300–400 m since the deposition of unit R5–R5B (see Supporting Information S1), suggesting slow slip rate of ~0.2 m/kyr (Figure 9), and it is possible this is due to accommodating transpressive slip out of the plane of seismic profile C.

4.3.2. Structural Evolution of Segment C Prism From Restoration

At 2 Ma (Stage 1, Figure 9a), our restoration results suggest that the fault C5 was the frontal thrust of Segment C. However, faults C1 and C3 may have already existed as faults that developed much earlier within the Chatham Rise TCT Wedge, but at Stage 1 were not yet activated by Hikurangi prism contraction.

The main period of fault propagation from the décollement at R7 occurred during the deposition of unit R4-R5 (between Stage 1 and 2, Figure 9), with seaward progression of the frontal thrust from C5 to C5_fs and then to C4. This corresponds to a relative advancement of ~19.3 km (and an approximate advancement rate of 19.3 km/Myr). Equal displacement of horizons between R4 and the TCT basement on faults C3 and C1 suggests these (pre-existing) faults were not active at this time (Stage 2, Figure 9b).

Propagation of the back-thrust C4_bt and development of the minor fault zone CMF3 probably occurred between the end of deposition of unit R4-R5 and the early stages of R3-R4 deposition (between Stage 2 and Stage 3), along with continued but minor propagation of C4. Following this, the frontal thrust advanced seaward, possibly jumping to a more deeply rooted pre-existing fault (C3). Faults C2 and C1 then likely propagated from similar structures within the Chatham Rise TCT wedge, with C1 ultimately acting as the frontal thrust. This represents a relative advancement of the frontal thrust of 30.4 km between Stage 2 and Stage 3, corresponding to an advancement rate of ~76 km/Myr. Minor fault zones CMF2 and CMF1 may have developed contemporaneously with this forward progression of the deformation front.

After Stage 3, the frontal thrust ceased to advance further seaward. During R0-R3 deposition (between Stage 3 and Stage 4), minor faulting in the vicinity of the deformation front developed, including the back-thrust C1_bt, and the minor fault zone CMF1 continues to be active. We note that CMF1 is part of the Hikurangi Channel thrust faults described by Crutchley et al. (2020). The geometry of unit R0-R3 in the landward limb of the fault C4 and C5 hanging-wall anticlines suggests some continued activity of these faults, however, slip is minimal with very little shortening occurring from Stage 4 to the present day (Stage 5) (Figures 9d and 9e). Within the uppermost sediments of R0-R3 deposition, there is some evidence of slumping occurring within the shallowest sediments, from older buried mass-transport deposits.
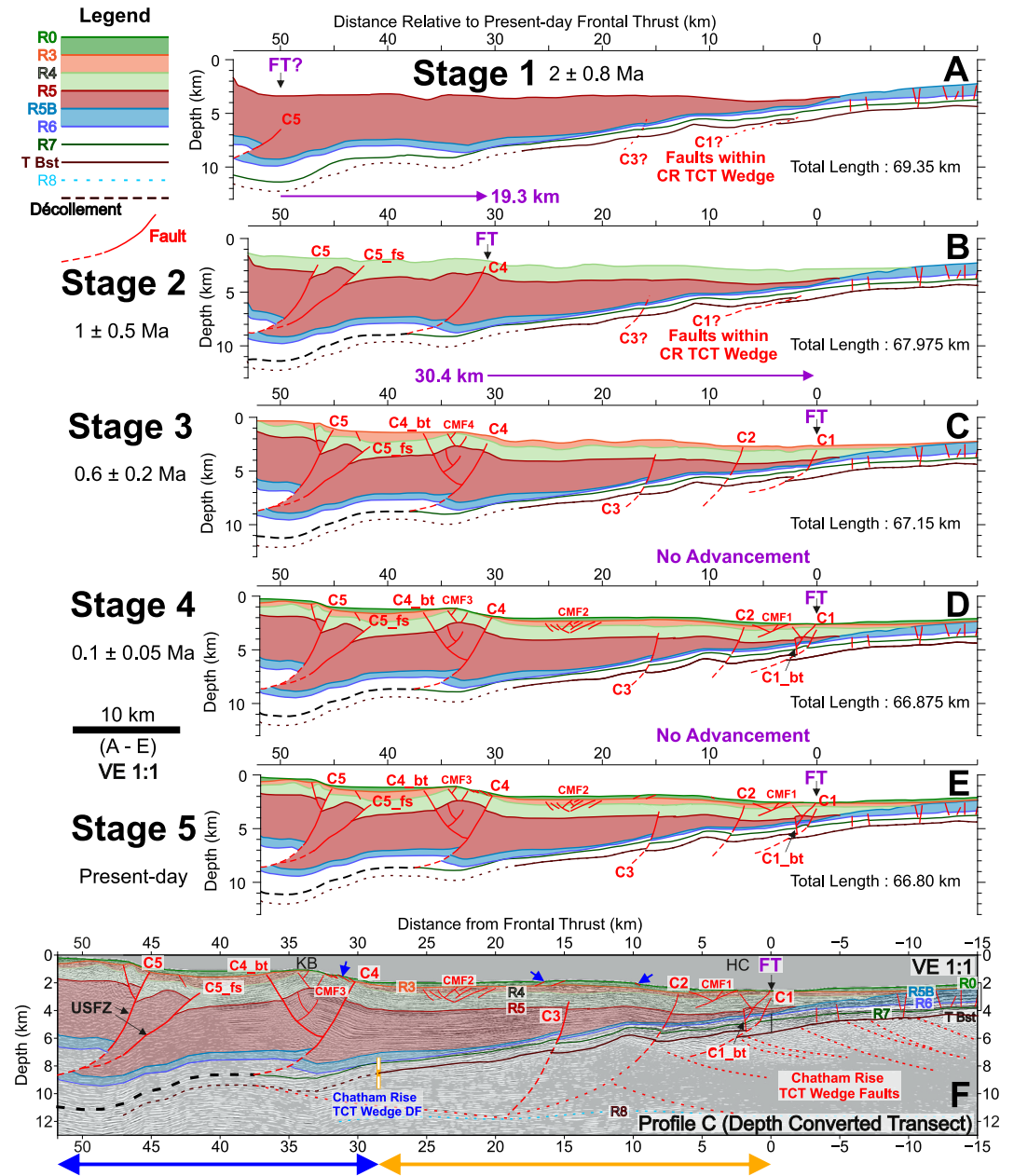
Figure 9. Retro-deformation restoration results for depth converted transect of seismic profile C. (a–e) The evolution of the prism since 2 Ma, where each stage shows the pre-deformed state at the end of deposition of the youngest sediment unit at each time. (f) Depth-converted seismic data showing interpretation. Colored lines numbered R0 to R8 are seismic marker horizons. Faults are red lines; numbers correspond to Figure 8. See Text S4 in Supporting Information S1 for full breakdown of retro-deformation steps. The blue arrow indicates extent of the prism unaffected by fault reactivation, and the orange arrow indicates extent of the prism which includes components of fault reactivation within the Chatham Rise TCT wedge.

The overall total relative advancement of the frontal thrust between Stage 1 and Stage 5 was 49.7 km, and accounting for errors in age, this corresponds to an advancement rate of between 17.8 and 41.4 km/Myr, with a best estimate of 24.85 km/Myr. However, the change in length of the restored section of Profile C from 69.35 km (original length L_0) at Stage 1–66.80 km (final length L_f) at the present-day (Stage 5) indicates a total estimated profile-parallel linear shortening of only ∼3.5%. This suggests the Profile C prism (Figure 9) has a deformation history distinct from the other two profiles, with rapid advancement of the frontal thrust, but minimal shortening since 2 Ma.
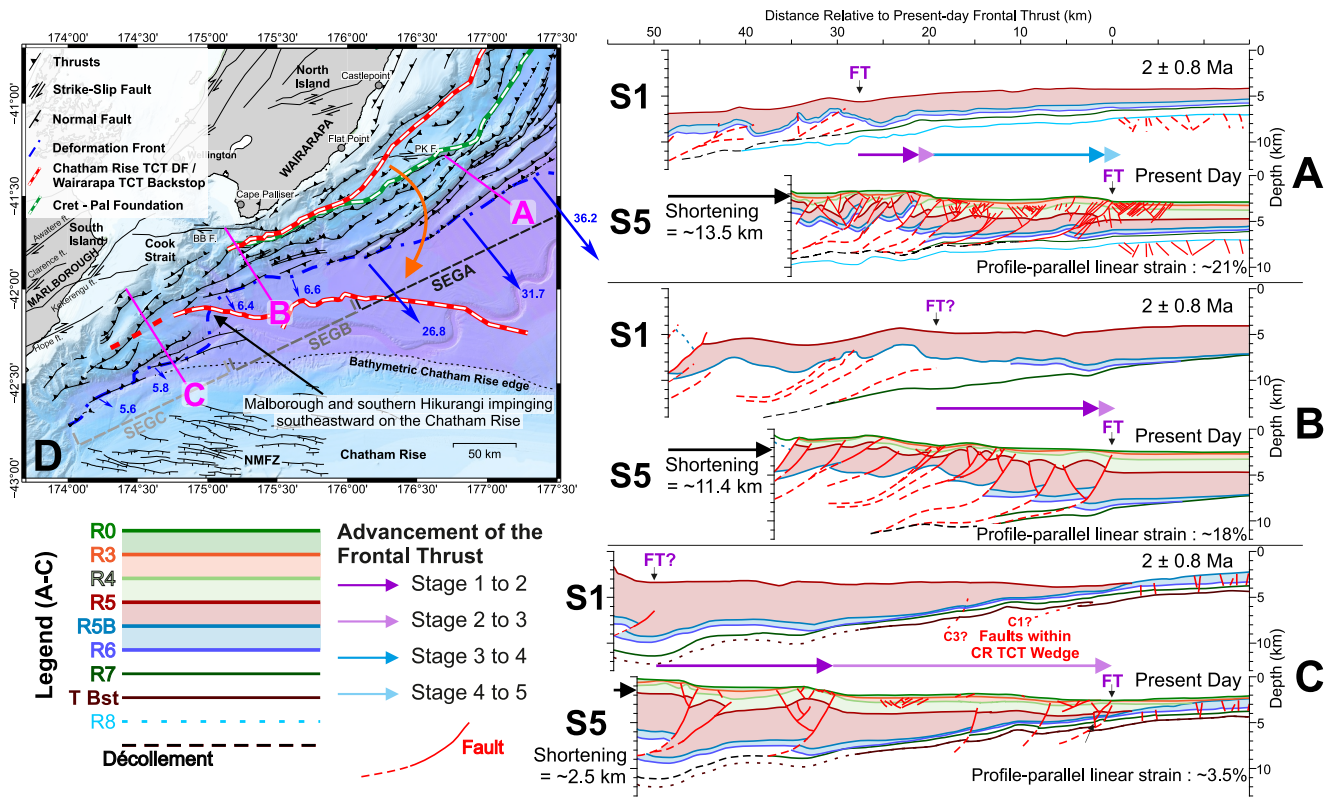
Figure 10. Compiled results of structural and restoration analysis. (a–c) Restored transects of Profiles A-C, showing Stage 1 (S1 2 ± 0.8 Ma) and Stage 5 (S5 Present Day). (d) Simplified map, showing location of the three Profiles. Orange arrow indicates schematic relative motion of the North Island as it rotates and impinges on the Chatham Rise.

5. Discussion

Our interpretation of the three seismic profiles integrated with existing interpretations along the margin suggests changes in the mechanical behavior of the southern Hikurangi accretionary prism over a 300 km stretch of the margin (Figure 10). We argue that each profile is representative of a distinct structural style, defining three tectonic segments. Here we discuss processes driving the tectonic segmentation and compare the observations at Hikurangi to other subduction margins.

5.1. The Chatham Rise as a Potential Control on Along-Margin Structural Changes

How factors such as plate convergence rate and obliquity, and sediment thickness on the incoming plate affect the nature of fault structure within accretionary prisms and subduction segmentation is the subject of much study and debate (Davis et al., 1983; von Huene & Scholl, 1991; Saffer & Bekins, 2002; Clift & Vannucchi, 2004; Wallace et al., 2009; Pedley et al., 2010; Heuret et al., 2012; Cook et al., 2014; McNeill & Henstock, 2014). Uniquely, at the Hikurangi margin, a Mesozoic terrane on the incoming Pacific Plate, that has been argued to act as a backstop to much of the contemporary prism (Bassett et al., 2022), is also underthrusting the frontal prism close to the southern termination of the subduction zone (Figure 10, segment C). We argue that both these factors have a significant impact on the mechanical behavior of the margin and its structure.

The Torlesse Composite Terrane (TCT) formed in the latest stages of Gondwana margin subduction in the Jurassic and Triassic, ending ~110–100 Ma (Begg et al., 2000; Laird & Bradshaw, 2004; Lee et al., 2002; Mortimer, 2004). The New Zealand portion of the Gondwana margin originally stretched along most of what is now the east coast of the North Island and Chatham Rise, forming between ~300 and 100 Ma (Mortimer, 2004). Subduction along the New Zealand portion of the Gondwana margin stalled at ~100 Ma after being choked by subduction of the relatively young, buoyant, Large Igneous Province volcanics of the Hikurangi Plateau (Davy et al., 2008). At this stage, and until as recently as 40 Ma, the Chatham Rise was aligned with the rest of the

Gondwana margin (Figure 3b; King, 2000; Bland et al., 2015). However, since 40 Ma, clockwise rotation of New Zealand's North Island, pivoting through the Marlborough region, has resulted in prominent bending of the accretionary terrane and presently an acute angle between the TCT rocks of the North Island (the Wairarapa TCT Backstop) and the Chatham Rise (the Chatham Rise TCT wedge) at the south-western extreme of the Hikurangi margin (Figures 3c and 10; King, 2000). In other words, whilst the Chatham Rise is on the Pacific plate, it comprises the TCT accretionary complex, and equivalent stratigraphy outcrops in southern Wairarapa (North Island) as the Early Cretaceous Pahaoa Group (Barker et al., 2009; Barnes & Korsch, 1990, 1991; Lee et al., 2002; Mountjoy & Barnes, 2011). Bassett et al. (2022) mapped the offshore position and seaward extent of these rocks beneath the inner Hikurangi margin (Wairarapa TCT backstop, Figures 1, 3 and 10), interpreting this as the backstop for the margin and potentially impacting frictional behavior and structural development of the forearc.

We suggest that the increasing proximity of the Hikurangi margin to the Chatham Rise TCT wedge toward the southwest and its ultimate impingement, partially underthrusting the TCT wedge is the primary control on the structural changes we observe between segments. We suggest the buoyant rocks of the Chatham Rise TCT wedge have the effect of stalling subduction and thus reducing margin-normal subduction velocity, alongside reductions in subduction velocity due to increased obliquity. Additional potential controls are changes in basement topography on the subducting plate and sediment thickness in the trench.

5.1.1. Segment A: Moderate Convergence Rate, Fluid-Rich Input Sediments, and Smooth Incoming Basement Topography (Most Similar to Central-Hikurangi-Type Subduction)

The buried Chatham Rise TCT wedge is too far south of the Hikurangi accretionary prism to influence the structure of the latter in Segment A (Figure 3). Margin-normal subduction velocity is high compared to Segments B and C (26–36 mm/yr compared to <7 mm/yr) (Figure 3). Margin-normal subduction velocity at Segment A is reduced compared to the central and northern parts of the Hikurangi margin, but this is the primarily the result of a gradual southwards reduction as the margin orientation becomes increasingly oblique to the PAC-AUS relative motion vector (Figure 1), and prism structure is very similar to the Central Hikurangi margin to the north (Figure 4; Barnes et al., 2010; Ghisetti et al., 2016; Gase et al., 2022). The Hikurangi prism of Segment A and the Central Hikurangi margin have extensive major thrust faults with an imbricate thrust wedge of seaward-vergent faults and distributed fault activity that acts to maintain the taper (Barnes et al., 2010; Ghisetti et al., 2016). This is typical of accretionary prisms with a smooth subducting plate, thick (>1 km) incoming sediments and moderate convergence (von Huene & Scholl, 1991; Clift & Vannucchi, 2004). As suggested by Barnes et al. (2010) for the Central Hikurangi margin, the low taper angle in Segment A implies it is poorly drained above an overpressured and/or weak décollement (Ellis et al., 2019; Saffer & Bekins, 2002).

In profile A, no faulting is identified within the incoming sediment sequence (excluding the proto-thrust zone and deep subducting normal faults), hence there is a lack of potential fluid conduits to drain the basal sediments, and we observe polarity reversal below reflector R7 and beneath the depth of décollement initiation (Figure 4) which may reflect trapped fluids. These observations, as well as low seismic velocities within the protoliths of the lower subducting sediments beneath the décollement (Arnulf et al., 2021; Crutchley et al., 2020; Plaza-Faverola et al., 2012, 2016), suggest the sediments may be fluid rich (Dean et al., 2010; Geersen et al., 2013; Stevens et al., 2021), and that fluids could be channeled along a weak décollement under the prism (Bangs et al., 1999; Brown et al., 2003; Morgan & Karig, 1995).

Our structural reconstruction within Segment A shows relatively fast advancement of the frontal thrust of ~13.75 km/Myr (between 9.8 and 22.9 km/Myr), and estimated shortening of 21% (~13.5 km) since 2 ± 0.8 Ma (and ~12.3 km since 1 ± 0.5 Ma). Note that these measurements exclude measurement of a major fault—A10— that lies beneath the Uruti Ridge (Figure 4). This amount of shortening is comparable to the result obtained by Ghisetti et al. (2016) on the central margin for the same time period (~13.3 km since 1 ± 0.5 Ma on seismic profile T03, Figure 1), but Ghisetti et al. (2016) estimate a higher advancement rate of the frontal thrust at the widest part of the Hikurangi margin of ~20–30 km/Myr. The difference in advancement rates is consistent with the south-westward decrease in margin-normal subduction velocity from the central margin and may be a response to this change. We acknowledge that our estimated rates of shortening only represent what is accommodated by the frontal accretionary prism of the margin, and additional shortening is accommodated by deformation within the Torlesse backstop to the west of Profile A and onshore (e.g., Nicol & Beavan, 2003). Nicol and Beavan (2003) and Nicol et al. (2007) document ~15 ± 5 km, and ~17 ± 3 km, of total margin-normal shortening accommodated

by deformation in the overriding plate excluding the frontal accretionary prism, respectively, since ∼5 Ma. These estimates of shortening equate to approximate rates of ∼2–5 m/Myr since 5 Ma. This is significantly lower than the rates for the frontal accretionary prism from this study (Profile A; ∼8–24 m/Myr since 1 ± 0.5 Ma) and from Ghisetti et al. (2016; profile T03; ∼9–27 m/Myr since 1 ± 0.5 Ma). Both Nicol and Beavan (2003) and Nicol et al. (2007) concluded that the backstop accommodated ∼20% of total plate convergence, which broadly agrees with the work presented in this paper.

Profile A appears to mark a boundary southwest of which major offshore strike-slip faults are present beneath the inner margin, coinciding with the Palliser-Kaiwhata Fault's eastern tip (Figure 3; Barnes et al., 1998). Thus, segment A lies within the subduction accretion—transpression zone identified by Watson et al. (2020). Southwest of Profile A, the prism also gradually narrows as a result of repeated right-stepping of the deformation front to the SW (Figure 3). The southwest boundary of Segment A (and start of Segment B) is marked by a drop in the margin-normal subduction velocity and the eastern termination of the Boo-Boo strike-slip fault (Figures 3 and 10; Mountjoy et al., 2009).

5.1.2. Segment B: Increased Proximity of the Chatham Rise, Sediment Thickness and Obliquity With Reduced Margin-Normal Subduction Velocity, and Increased Strike-Slip Faulting

The increasing proximity of the Chatham Rise to the southern Hikurangi margin results in along-strike changes in margin structure between segments A and B. Despite little change in PAC-AUS relative plate motion vector (Beavan et al., 2002), the increasing transition southwards from subduction to transform tectonics (Barnes et al., 1998; Wallace, Barnes, et al., 2012) generates along-strike changes in margin structure. The key regional drivers are the southward change from subducting oceanic rocks of the Hikurangi Plateau to colliding continental rocks of the Chatham Rise. Reduced plate convergence results largely from clockwise rotation of the eastern North Island coupled with the transfer of displacement to the strike-slip faults of eastern Marlborough and Cook Strait (Figures 1 and 3). Despite reduced convergence rate on the subduction interface and increasing obliquity of plate motion, the convergence direction at the trench remains orthogonal (Wallace et al., 2004, 2012a, 2018). The reduced subduction rate at the trench coincides with a narrowing forearc controlled by right-stepping of the deformation front to the southwest through both segments A and B.

The Boo-Boo fault at the landward edge of the Segment B prism accommodates ∼20% of the total plate motion (Seebeck et al., 2023; Wallace, Barnes, et al., 2012) (Figures 3 and 10), and was considered by Barnes and Audru (1999) to have developed since 1 Ma. This development is broadly coincident with the cessation of advancement of the frontal thrust in Profile B (Figure 7). Our results suggest that before 1 Ma, the overall relative advancement rate of the frontal thrust at Segment B (∼17.8 km/Myr) was reasonably close to the average rate at Segment A (∼13.75 km/Myr) and the central margin from 2 Ma to present (20–30 km/Myr) (Ghisetti et al., 2016), but has ceased since, approximately coincident with development of this significant strike-slip fault. We suggest a possible explanation is the timing of impingement of the Chatham Rise TCT wedge on the Hikurangi subduction zone at Segment C at ∼1 Ma (see below). Since 1 Ma, margin-normal shortening has been accommodated by continued activity on faults within the Segment B prism rather than forward advancement of the frontal thrust (Figure 7). This lack of advancement and continued fault activity has produced the steeper taper angle of the Segment B prism (∼8°) compared to that of Segment A (∼5°).

5.1.3. Segment C: Impingement of Southern Hikurangi on the Chatham Rise TCT Wedge and Reactivation of Terrane Faulting

We define the boundary between Segments B and C as the impingement point of the Hikurangi margin on the TCT wedge and where there is a substantial, seaward outstepping of the contemporary deformation front (Figures 3 and 10).

We infer that major thrust C4 (the 'Kekerengu Bank Fault', Barnes et al., 1998) and potentially faults landward of this point detach into the décollement hosted at Reflector R7 (Crutchley et al., 2020). Seaward of fault C4, the presence and position of a potential décollement is less clear.

Our interpretation is that the top of the Chatham Rise TCT wedge extends at least 25 km landward of fault C1, where we place the present-day deformation front, close to the position of fault C4 (Figure 8). We therefore subdivide Profile C into two zones, approximately demarcated by the position of fault C4. Landward, and inclusive

of, fault C4 is a zone which represents Hikurangi prism unaffected by fault reactivation, comparable to ongoing processes in Segment A (and the central-Hikurangi margin); seaward of fault C4 is a zone which includes potential components of fault reactivation within the Chatham Rise TCT Wedge (see blue and orange arrows on Figures 8 and 9). Within the latter zone, we suggest a number of options for the nature of faulting. Consistent with the interpretation presented in this paper: option (a) is that faults C1–C3 are reactivated Chatham Rise TCT wedge faults that cut Reflector R7, that there is no active Hikurangi prism décollement beneath them, and that they represent only local shortening of the Pacific Plate; or option (b) faults C1–C3 are reactivated Chatham Rise TCT wedge faults that cut Reflector R7, but there is an active Hikurangi prism décollement beneath them which has stepped down to a level deeper than R7. Option 1 presents C4 as a seaward limit of the Hikurangi prism, whereas should option 2 be more accurate, then the active Hikurangi prism extends seaward to C1. Option two is comparable to the interpretation in Crutchley et al. (2020).

Other possibilities require a different interpretation of the seismic data (hence why faults C1–C3 are dashed below Reflector R7 in Figures 8 and 9). One such option (c) is that fault C1 marks the Hikurangi deformation front, but the fault does not cut Reflector R7, and the décollement extends along R7 from fault C4 to C1. In this scenario, faults C2 and C3 would be blind and not propagate shallower than R7 but would be reactivated Chatham Rise TCT wedge faults facilitating contraction of the Chatham Rise TCT wedge beneath the décollement. The final option (d) would involve no fault reactivation within the Chatham Rise TCT wedge: faults C1–C3 do not cut Reflector R7, the décollement extends along R7 from fault C4 to C1, and apparent relief and faulting beneath R7 is entirely inherited from deformation in the Mesozoic prior to cessation of Gondwana subduction.

For all of these options, fault C1 marks the seaward extent of deformation that, if not facilitates, is related to subduction at the Hikurangi margin. Therefore, our restoration results are broadly applicable to all options 1–4. These results suggest that prior to 1 Ma, during the period of "normal" Hikurangi prism subduction that produced fault C4, the overall relative advancement rate of the frontal thrust at Segment C was ~19.3 km/Myr, comparable to that for Segment B during the same period and the overall advancement for the central part of the margin from 2 Ma to the present day (20–30 km/Myr, Ghisetti et al., 2016). This advancement rate is also comparable to the present-day margin-normal subduction velocity at Segment A (~30 mm/yr = 30 km/Myr). We suggest that the 2-1 Ma advancement rate of the frontal thrust at Segment C reflects a past margin-normal subduction velocity similar to what is presently observed for Segment A, since Segment A represents "normal" Hikurangi subduction but where the orientation of the deformation front is similarly oblique to the PAC-AUS relative motion vector. Therefore, the Hikurangi margin would have impinged on the Chatham Rise TCT wedge deformation front, when the Hikurangi deformation front would have been at fault C4, approximately 1 Ma. This process stalled, or at least significantly slowed down, subduction and resulted in the initiation of, and transfer of strain to, the Boo-Boo fault. Thus, it has far-field effects on the processes occurring within Segment B. We suggest this is also supported by the relatively small amount of shortening we estimate across Profile C, which is consistent with kinematic models that suggest a reduction of convergence and increased transpression and strike-slip faulting (Barnes et al., 1998; Wallace et al., 2012a) (Figure 1). We suggest that Profile B may be representative of earlier stages of subduction at Segment C, prior to the impingement of the margin on the Chatham Rise TCT wedge, and that Segment B will evolve into a state similar to Segment C should there be continued impingement and underthrusting of the Chatham Rise TCT wedge.

5.2. Controls of Changing Hikurangi Forearc Structure and Comparison to Other Subduction Zone Margins

Many studies have examined key controls on the styles of forearc deformation. Parameters include: basement topography and sediment thickness and composition, with the two often linked (e.g., McNeill & Henstock, 2014; Westbrook et al., 1982), stratigraphic position at which the décollement forms within the incoming sediments (e.g., Han et al., 2017; Moore et al., 1988, 1990; Shipley & Moore, 1986), presence and position of a strong backstop (e.g., Byrne et al., 1993; Kopp & Kukowski, 2003; Tsuji et al., 2015), and margin-normal subduction velocity and the obliquity of convergence. Resulting structural segmentation along accretionary margins is common (e.g., Laigle et al., 2013; MacKay et al., 1992; McNeill & Henstock, 2014; Tsuji et al., 2014). There are particular similarities in the variation of subduction configuration between the Hikurangi margin and Sunda margin (SE Indian Ocean), for example, between North to Central Hikurangi and West Java to South Sumatra, and between south-Central to Southern Hikurangi and Central to North Sumatra: The key changes in along-strike variation at these margin sections and a comparison between them are summarized in Table 2. Particular driving mechanisms for the Hikurangi margin are explored in the following sections.

Table 2
Comparison of Subduction Configuration at the Hikurangi Margin With Parts of the Sunda Margin

Changing aspects of subduction configuration	North to central Hikurangi (NE to SW changes)	West Java to South Sumatra (SE to NE changes)	South-central Hikurangi to South Hikurangi (NE to SW changes)	North-central to north Sumatra (SE to NE changes)
Approximate total distance (km)	350	1,100	300	1,100
Plate Motion Obliquity[a]	From 30° to 60°	From orthogonal to 20°	From 60° to 85° (margin-parallel)	From 24° to 70°
Margin-Normal Subduction Velocity (mm/yr)[b]	From 61 to 35[2]	From 64 to 47[10]	From 35 to <6[2]	From 43 to 35
Structure of incoming plate	Change from rough basement topography scattered with seamounts and thin sedimentary cover, to smooth basement with moderate sediment cover[3,6]	Change from rough basement topography scattered with seamounts and thin sedimentary cover, to smooth basement with moderate sediment cover[10]	Change from smooth basement with moderate sediment cover to very thick sediments onlapping onto flank of incoming ancient accretionary complex (which increases in proximity) and associated fault structure	Change from smooth basement with moderate sediment cover to very thick sediments that are pervasively deformed by intraplate faulting[10]
Trench sediment thickness (km)[c]	From 0 to 3[3]	Variable between 1 and 2[10]	From 4.5 to >6	From 2.5 to 5[10]
Taper[d]	From >10° (α = >3°, β = >8°) to <4° (α = 1–2°, β = 2–3.5°)[3,8]	From ~10° (α = 3.5°, β = 7°) to ~7° (α = 2.5–3.8°, β = 1–7°)[10]	From ~5° (α = ~2.2°, β = 3°) to >10° (α = ~3.3°, β = 7°)	From ~6 to 8° (α = ~2.4°, β = 0–8°) to >10° (α = ~3.5°, β = 5–8°)[10]
Prism Width (km)	From 60 to 150[3,7,8]	From 110 to 140	From 70 to 140 to ~50	From 125 to 165 (but variable between 100 and 165)
Thrust Vergence	Seaward[3]	From seaward to mixed[10]	Seaward (but with back-thrusts, somewhat more prominent to the south)	From mixed to Landward[10]
Similarities	Similar variation in subduction velocity, structure of the incoming plate, sediment thickness within the trench and prism morphology		Comparable changes in obliquity, initially similar incoming basement topographies and trench sediment thickness and similar changes in overall prism taper	
Differences	Subduction erosion occurs in North Hikurangi, but not at West Java (although is apparent further east along-strike of the Sunda margin). Changes occur over a much larger distance at the Sumatra-Andaman margin		Significantly greater reduction in margin-normal subduction velocity at Hikurangi occurring over much smaller distance. The North Sumatra prism exhibits a steep toe and plateau geometry as well as extensive occurrence of landward vergent thrusts, which are not observed at Hikurangi	
Potential driving mechanisms	Decreasing roughness of the incoming basement topography and increasing sediment cover	Decreasing roughness of the incoming basement topography and increasing sediment cover	Increasing proximity of the Chatham Rise accretionary complex to the subduction zone and decreasing subduction velocity	Changes in incoming sediment properties controlling the position of the décollement and cohesive strength of accreted materials

Note. 1. Wallace et al. (2004); 2. Wallace et al. (2018); 3. Barker et al. (2009); 4. Lewis et al. (1998); 5. Wallace, Barnes, et al. (2012); 6. Bell et al. (2010); 7. Barnes et al. (2010); 8. Ghisetti et al. (2016); 9. Barnes et al. (2018); 10. McNeill and Henstock (2014). [a]Angle of incidence between absolute plate motion in degrees from orthogonal convergence (e.g., McNeill & Henstock, 2014) and does not account for strain partitioning (e.g., due to strike-slip activity). [b]Orthogonal convergence vector (mm/yr). [c]At present day deformation front. [d]Within 40 km of the deformation front for Segments A-C.

5.2.1. The Role of the Proximal Input Section

Both the Hikurangi and Sunda margins have large sections with contrasting input materials along-strike, from thick sediment cover overlying low subducting basement topography to thin sediment cover over basement with significant topographic variation (seamounts). Therefore, differences in their prism structure and the position of the décollement along and between these margin sections could be explained by the characteristics of the input section (e.g., Underwood, 2007). The Hikurangi margin is particularly unusual where Cretaceous volcaniclastics

of the Hikurangi Plateau Large Igneous Province reach depths of >9 km below the seafloor in the southern trench (Plaza-Faverola et al., 2012). Above this the sequence includes sedimentary rocks of the Gondwana subduction trench, which lay oceanwards of the Chatham Rise TCT wedge (Bland et al., 2015; Davy et al., 2008) and the North Island TCT wedge now representing the backstop to the modern Hikurangi prism (Barnes & Korsch, 1990, 1991; Bassett et al., 2022; Lee et al., 2002). The top of the Chatham Rise TCT wedge, which is much shallower than the Hikurangi Plateau in the south, essentially marks the transition from oceanic to continental incoming basement. Further north the sedimentary sequence between the Hikurangi Plateau and reflector R7 is thinner (Gase et al., 2022), and the Chatham Rise TCT wedge is not a feature of the local incoming plate.

On the Hikurangi margin, trench sediment thickness generally increases southwards along the margin (Table 1). In South Hikurangi (this study) the trench sediment thickness is greatest in Segment B, up to 5.5 km of clastic trench wedge and 9 km of total sediment (Plaza-Faverola et al., 2012). Further north at Central Hikurangi the correlative sequences reach 3 and 4.5 km respectively (Ghisetti et al., 2016; Plaza-Faverola et al., 2016). In spite of this big difference in sediment thickness and the increasing role of the Chatham Rise southwards, the Hikurangi décollement forms in the same stratigraphic position on the southern and central Hikurangi margin—at Reflector seven interpreted to be the top of a condensed, low permeability layer of nannofossil chalk and interbedded mudstones overlying lower velocity MES sediments, interpreted as fluid-rich and over-pressured clastics (Barnes et al., 2018; Crutchley et al., 2020; Ghisetti et al., 2016; Plaza-Faverola et al., 2016). At the southwest extreme of the margin (Segment/Profile C) where it impinges on the and the Chatham Rise TCT wedge starts to underthrust, the stratigraphic level of the décollement is less clear as the style of deformation changes to incorporate reactivated faults within the Chatham Rise TCT wedge. The thickness of the sediments that underly Reflector 7 vary from 500 to 1,500 m along the southern and central parts of the margin (Gase et al., 2022), therefore, sedimentary layer properties exhibit a stronger control over where the décollement initiates here than sediment thickness and specific depth of initiation. In contrast, as incoming sediment thins between Central and North Hikurangi, basement topography exerts more control on the décollement position with the décollement forming at the top of basement particularly where seamounts are being subducted (Barnes et al., 2020; Gase et al., 2022; Wallace et al., 2019).

Comparing with the Sunda margin, at North Sumatra where input sediments are thick, the décollement is interpreted to form at a fluid-rich over-pressured layer (Dean et al., 2010) at the boundary between pelagic and hemipelagic muds and overlying Nicobar Fan sediments (McNeill et al., 2017). This appears to persist along this part of the margin and is a layer comparable to R7 for the Central and Southern Hikurangi margin, that is, specific sedimentary layer properties controlling the position of the décollement. In Central Sumatra, thinner sediments on the incoming plate result in more interaction with the oceanic basement and the décollement commonly initiates at the basement-sediment interface (e.g., Cook et al., 2014); the same scenario as in North Hikurangi.

As on the Sunda margin (Table 2; McNeill & Henstock, 2014), at Hikurangi there is a general correlation between taper angle and prism width and incoming sediment thickness, particularly between North and Central Hikurangi. However, on the South Hikurangi margin, the approaching and locally underthrusting Chatham Rise TCT wedge also plays a key role and there are abrupt deviations from this correlation. In Segment B, with the thickest trench sediment thickness (Table 1), the prism width is actually small and the taper angle moderate, corresponding to cessation of advancement of the prism and continued activity on older thrust faults (a reflection of the processes discussed in Section 5.1.2). In Segment C where the TCT wedge is underthrusting, the sediment thickness overlying basement (top of the TCT wedge) is less than in Segment B (where basement at the deformation front is still the top of the Hikurangi Plateau), but the prism is wider due to the prism jumping outboard, possibly as subducting faults are now reactivated. If actual prism widths are compared, in spite of similar clastic trench wedge thicknesses, (up to 3.5–5.5 km in South Hikurangi; ~5 km in North Sumatra), the prism at Southern Hikurangi is much narrower (~40–70 km compared to 120–180 km). Globally where accretion dominates, there is a strong correlation between sediment input thickness and prism width (e.g., von Huene & Scholl, 1991; McNeill & Henstock, 2014).

5.2.2. The Role of Convergence Rate and Obliquity

In the case of Hikurangi, we note that input properties and convergence rate and obliquity are linked, as the composition and structure of the Pacific Plate has ultimately controlled the progression of subduction, rotation of the North Island relative to the South Island, convergence rate and the transition from subduction to transpression. However, in this section we explore direct impacts of changing convergence and obliquity.

Toward the southwest along the Hikurangi margin, obliquity and strike-slip faulting increase and margin-normal subduction velocity decreases. Margin-normal subduction velocity at southern Hikurangi is extremely low (5.6–6.6 mm/yr, Figure 3, Table 1) (Wallace, Barnes, et al., 2012, 2018) and plate convergence is highly oblique. There is comparable convergence obliquity along the northernmost parts of the Sunda subduction zone and in Fiordland, New Zealand. On the Sunda margin, major strike-slip faults enable complete strain partitioning but margin-normal subduction velocity, though low, is substantially higher (21–23 mm/yr) than at Southern Hikurangi (McNeill & Henstock, 2014). In many obliquely convergent margins, strike-slip faults form at the rear/landward edge of the prism (backstop edge) and at the position of the arc, for example, Nankai and Sumatra. The Southern Hikurangi margin is relatively unusual in terms of its strike-slip faulting because a) the plate boundary is transitioning from subduction to transform/transpression and b) the Mesozoic Chatham Rise TCT wedge plays a role in forearc structure. Point (a) is a possible reason for margin-parallel strike-slip faulting also forming within the middle of the accretionary prism (Wallace, Barnes, et al., 2012) rather than at its rear, and point (b) results in forearc segmentation (Segments A and B) due to impingement on and local underthrusting of the Chatham Rise TCT wedge beneath the Marlborough margin.

In general, as margin-normal subduction velocity rates decrease between Central and Southern Hikurangi, the accretionary prism narrows, and this is accomplished with stepping of the deformation front and discontinuity of the frontal thrust. The general trend is comparable to the Northernmost Sunda margin where margin-normal subduction velocity and prism width are significantly reduced relative to the North Sumatra and Nicobar margins. However, there are some deviations from this trend at Hikurangi, for example, in Segments B and C, due to the complexities of propagation of the active prism front responding to impingement on the Chatham Rise. Overall, as the Hikurangi plate boundary transitions from subduction to transform, strain is partitioned, with increasing activity on strike-slip faults and reduced orthogonal convergence resulting in reduced tectonic shortening and width of the prism.

Ultimately, many forearc parameters at both the Hikurangi and Sunda margins (and other global margins) are a combined function of input thickness/properties and convergence parameters. However, in Sunda, sediment thickness generally dominates (McNeill & Henstock, 2014), whereas in Hikurangi, convergence parameters (driven by the large-scale Pacific Plate properties) appear to dominate. We suggest that at Southern Hikurangi, prism structure is most likely controlled by the approach to, and impingement on, the continental Chatham Rise, resultant reduction in margin-normal subduction velocities, and strike-slip faulting in the prism interior. There is an element of positive feedback between these factors: impingement on the Chatham Rise results in a significant reduction in margin-normal subduction velocity; strike-slip faulting within the Hikurangi forearc initiated in response to the relative plate motion; and these strike-slip faults act to further reduce margin-normal subduction velocity at the Hikurangi trench, which is a control on the prism structure.

6. Conclusions

- The Southern Hikurangi margin can be divided into three segments with contrasting accretionary prism morphologies and prism growth rates. These changes can be related primarily to a southwards change from oceanic subduction to continental collision and transform faulting. A key factor is the impingement of the Hikurangi margin on the continental Chatham Rise as the incoming plate subducts. This transforms the subducting plate basement and it becomes the Mesozoic Torlesse Composite Terrain (TCT) accretionary wedge formed by subduction at the Gondwana margin >100 Ma. There are also related differences in the velocity of subduction (orthogonal component of plate convergence), and strike-slip faulting in the prism interior.
- The northeastern segment of the Southern Hikurangi margin (Segment A) is characterized by a moderately wide prism (70 km) with a low taper angle (~5°), related to a smooth incoming oceanic basement overlain by undeformed sediments and moderate convergence rate. Significant margin-normal crustal shortening (~20% over the reconstructed prism section) over the last ~1 Ma has been accommodated by outward growth of the prism via seaward-vergent thrusting, which is unaffected by any far-field impacts of impingement on the Chatham Rise TCT wedge.
- The central segment of the Southern Hikurangi margin that straddles the southern Cook Strait (Segment B) is characterized by a narrow prism (<40 km) with a moderate taper of ~8°, low convergence rate and significant strike-slip faulting in the prism interior, due to strain partitioning. Outward prism growth (occurring by seaward-vergent thrusting with related back-thrusting) effectively ceased at ~1 Ma, approximately coincident

- with development of the strike-slip Boo Boo Fault in southern Cook Strait, and potentially also impingement of Hikurangi margin on the Chatham Rise TCT wedge.
- The southwestern-most segment of the Southern Hikurangi margin (Segment C) is characterized by a fairly narrow prism (~50 km) with a high taper angle of >10°. This segment has a low convergence rate and reduced shortening across the outer prism. The deformation front has migrated rapidly seaward, where contraction of the prism is facilitated by reactivation of pre-existing fault structures within the converging Chatham Rise TCT wedge, rather than outward propagation of newly formed thrust from the décollement.
- The configuration of the southern Hikurangi margin has a number of similarities to the other margins, including Sunda and Nankai. For example, along-strike increases in sediment thickness, increasing obliquity and decreasing margin-normal subduction velocity, and decreasing roughness of the incoming basement impacting forearc morphological changes along strike. However, there are key differences, specifically, at the Sunda margin the prism structure is generally dominated by sediment thickness on the incoming plate, whereas at the Hikurangi margin, changes in convergence driven by large scale properties of the incoming plate appear to dominate.

Data Availability Statement

Bathymetry data were provided by New Zealand's National Institute of Water and Atmospheric Research (NIWA) which is available through Zenodo (https://doi.org/10.5281/zenodo.10359823) (Mackay, 2023). Marine multi-channel seismic from the SHIRE project are available through the Marine Geoscience Data System (http://www.marine-geo.org/collections/) (Bangs et al., 2018). The PEG09 seismic data are available from New Zealand Petroleum and Minerals, a division of MBIE (https://geodata.nzpam.govt.nz/survey/1192170815; PEG09, 2009). This work was carried out in part using the MOVE Suite structural modelling and analysis toolkit from PE Limited, and also in part using Petrel subsurface software from SLB (Petrel, 2019).

References

Allmendinger, R. W. (1998). Inverse and forward numerical modeling of trishear fault-propagation folds. *Tectonics*, *17*(4), 640–656. https://doi.org/10.1029/98TC01907

Arnulf, A. F., Biemiller, J., Lavier, L., Wallace, L. M., Bassett, D., Henrys, S., et al. (2021). Physical conditions and frictional properties in the source region of a slow-slip event. *Nature Geoscience*, *14*(5), 334–340. https://doi.org/10.1038/s41561-021-00741-0

Ballance, P. F. (1976). Evolution of the upper cenozoic magmatic arc and plate boundary in northern New Zealand. *Earth and Planetary Science Letters*, *28*(3), 356–370. https://doi.org/10.1016/0012-821X(76)90197-7

Bangs, N., vanAvendonk, H., Wallace, L., Proctor, W., Pilarczyk, J., Marshall, J., et al. (2018a). Multi-channel seismic shot data from the hikurangi subduction margin collected during Langseth cruise MGL1708 (2017). [Dataset]. *MGDS*. https://doi.org/10.1594/IEDA/324462

Bangs, N., vanAvendonk, H., Wallace, L., Proctor, W., Pilarczyk, J., Marshall, J., et al. (2018b). Raw seismic navigation data (P1 format) from the hikurangi subduction margin collected during R/V Marcus G. [Dataset]. *Langseth expedition MGL1708*. https://doi.org/10.1594/IEDA/324459

Bangs, N. L. B., Moore, G. F., Gulick, S. P. S., Pangborn, E. M., Tobin, H. J., Kuramoto, S., & Taira, A. (2009). Broad, weak regions of the Nankai Megathrust and implications for shallow coseismic slip. *Earth and Planetary Science Letters*, *284*(1–2), 44–49. https://doi.org/10.1016/j.epsl.2009.04.026

Bangs, N. L. B., Shipley, T. H., Moore, J. C., & Moore, G. F. (1999). Fluid accumulation and channeling along the northern Barbados Ridge decollement thrust. *Journal of Geophysical Research*, *104*(B9), 20399–20414. https://doi.org/10.1029/1999jb900133

Barker, D. H. N., Sutherland, R., Henrys, S., & Bannister, S. (2009). Geometry of the Hikurangi subduction thrust and upper plate, North Island, New Zealand. *Geochemistry, Geophysics, Geosystems*, *10*(2). https://doi.org/10.1029/2008GC002153

Barnes, P. M., Lamarche, G., Bialas, J., Henrys, S., Pecher, I., Netzeband, G. L., et al. (2010). Tectonic and geological framework for gas hydrates and cold seeps on the Hikurangi subduction margin, New Zealand. *Marine Geology*, *272*(1–4), 26–48. https://doi.org/10.1016/j.margeo.2009.03.012

Barnes, P. M. (1994). Inherited structural control from repeated cretaceous to recent extension in the North Mernoo Fault Zone, western Chatham Rise, New Zealand. *Tectonophysics*, *237*(1–2), 27–46. https://doi.org/10.1016/0040-1951(94)90157-0

Barnes, P. M., & Audru, J. C. (1999). Quaternary faulting in the offshore flaxbourne and Wairarapa basins, southern Cook Strait, New Zealand. *New Zealand Journal of Geology and Geophysics*, *42*(3), 349–367. https://doi.org/10.1080/00288306.1999.9514851

Barnes, P. M., De Lépinay, B. M., Collot, J. Y., Delteil, J., & Audru, J. C. (1998). Strain partitioning in the transition area between oblique subduction and continental collision, Hikurangi margin, New Zealand. *Tectonics*, *17*(4), 534–557. https://doi.org/10.1029/98TC00974

Barnes, P. M., Ghisetti, F. C., Ellis, S., & Morgan, J. K. (2018). The role of protothrusts in frontal accretion and accommodation of plate convergence, Hikurangi subduction margin, New Zealand. *Geosphere*, *14*(2), 440–468. https://doi.org/10.1130/GES01552.1

Barnes, P. M., & Korsch, R. J. (1990). Structural analysis of a middle Cretaceous accretionary wedge, Wairarapa, New Zealand. *New Zealand Journal of Geology and Geophysics*, *33*(2), 355–375. https://doi.org/10.1080/00288306.1990.10425693

Barnes, P. M., & Korsch, R. J. (1991). Melange and related structures in Torlesse accretionary wedge, Wairarapa, New Zealand. *New Zealand Journal of Geology and Geophysics*, *34*(4), 517–532. https://doi.org/10.1080/00288306.1991.9514487

Barnes, P. M., & Mercier De Lépinay, B. (1997). Rates and mechanics of rapid frontal accretion along the very obliquely convergent southern Hikurangi margin, New Zealand. *Journal of Geophysical Research B: Solid Earth*, *102*(B11), 24931–24952. https://doi.org/10.1029/97jb01384

Barnes, P. M., Wallace, L. M., Saffer, D. M., Bell, R. E., Underwood, M. B., Fagereng, A., et al. (2020). Slow slip source characterized by lithological and geometric heterogeneity. *Science Advances*, *6*(13). https://doi.org/10.1126/sciadv.aay3314

Bartlow, N. M., Wallace, L. M., Beavan, R. J., Bannister, S., & Segall, P. (2014). Time-dependent modeling of slow slip events and associated seismicity and tremor at the Hikurangi subduction zone, New Zealand. *Journal of Geophysical Research: Solid Earth*, *119*(1), 734–753. https://doi.org/10.1002/2013JB010609

Bassett, D., Arnulf, A., Henrys, S., Barker, D., Van Avendonk, H., Bangs, N., et al. (2022). Crustal structure of the hikurangi margin from SHIRE seismic data and the relationship between forearc structure and shallow megathrust slip behavior. *Geophysical Research Letters*, *49*(2). https://doi.org/10.1029/2021GL096960

Beavan, J., Tregoning, P., Bevis, M., Kato, T., & Meertens, C. (2002). Motion and rigidity of the Pacific plate and implications for plate boundary deformation. *Journal of Geophysical Research*, *107*(B10), ETG191–ETG1915. https://doi.org/10.1029/2001jb000282

Begg, J. G., Johnston, M. R., & McSaveney, E. (2000). Geology of the Wellington area.

Bell, R., Sutherland, R., Barker, D. H. N., Henrys, S., Bannister, S., Wallace, L., & Beavan, J. (2010). Seismic reflection character of the Hikurangi subduction interface, New Zealand, in the region of repeated Gisborne slow slip events. *Geophysical Journal International*, *180*(1), 34–48. https://doi.org/10.1111/j.1365-246X.2009.04401.x

Bland, K. J., Uruski, C. I., & Isaac, M. J. (2015). Pegasus Basin, eastern New Zealand: A stratigraphic record of subsidence and subduction, ancient and modern. *New Zealand Journal of Geology and Geophysics*, *58*(4), 319–343. https://doi.org/10.1080/00288306.2015.1076862

Boston, B., Moore, G. F., Jurado, M. J., & Sone, H. (2016). Deformation of the Nankai Trough inner accretionary prism: The role of inherited structures. *Geochemistry, Geophysics, Geosystems*, *17*(2), 485–500. https://doi.org/10.1002/2015GC006185

Brown, K. M., Kopf, A., Underwood, M. B., & Weinberger, J. L. (2003). Compositional and fluid pressure controls on the state of stress on the Nankai subduction thrust: A weak plate boundary. *Earth and Planetary Science Letters*, *214*(3–4), 589–603. https://doi.org/10.1016/S0012-821X(03)00388-1

Byrne, D. E., Wang, W.-h., & Davis, D. M. (1993). Mechanical role of backstops in the growth of forearcs. *Tectonics*, *12*, 123–144. https://doi.org/10.1029/92TC00618

Clark, K. J., Hayward, B. W., Cochran, U. A., Grenfell, H. R., Hemphill-Haley, E., Mildenhall, D. C., et al. (2011). Investigating subduction earthquake geology along the southern Hikurangi margin using palaeoenvironmental histories of intertidal inlets1. *New Zealand Journal of Geology and Geophysics*, *54*(3), 255–271. https://doi.org/10.1080/00288306.2011.562903

Clark, K. J., Hayward, B. W., Cochran, U. A., Wallace, L. M., Power, W. L., & Sabaa, A. T. (2015). Evidence for past subduction earthquakes at a plate boundary with widespread upper plate faulting: Southern hikurangi margin, New Zealand. *Bulletin of the Seismological Society of America*, *105*(3), 1661–1690. https://doi.org/10.1785/0120140291

Clift, P., & Vannucchi, P. (2004). Controls on tectonic accretion versus erosion in subduction zones: Implications for the origin and recycling of the continental crust. *Reviews of Geophysics*, *42*(2). https://doi.org/10.1029/2003RG000127

Collot, J. Y., Delteil, J., Lewis, K. B., Davy, B., Lamarche, G., Audru, J.-C., et al. (1996). From oblique subduction to intra-continental transpression: Structures of the southern Kermadec-Hikurangi margin from multibeam bathymetry, side-scan sonar and seismic reflection. *Marine Geophysical Research*, *18*(2–4), 357–381. https://doi.org/10.1007/BF00286085

Collot, J. Y., Marcaillou, B., Sage, F., Michaud, F., Agudelo, W., Charvis, P., et al. (2004). Are rupture zone limits of great subduction earthquakes controlled by upper plate structures? Evidence from multichannel seismic reflection data acquired across the northern Ecuador-southwest Colombia margin. *Journal of Geophysical Research*, *109*(B11), 1–14. https://doi.org/10.1029/2004JB003060

Cook, B. J., Henstock, T. J., McNeill, L. C., & Bull, J. M. (2014). Controls on spatial and temporal evolution of prism faulting and relationships to plate boundary slip offshore north-central Sumatra. *Journal of Geophysical Research: Solid Earth*, *119*(7), 5594–5612. https://doi.org/10.1002/2013JB010834

Crutchley, G. J., Klaeschen, D., Henrys, S. A., Pecher, I. A., Mountjoy, J. J., & Woelz, S. (2020). Subducted sediments, upper-plate deformation and dewatering at New Zealand's southern Hikurangi subduction margin. *Earth and Planetary Science Letters*, *530*, 115945. https://doi.org/10.1016/j.epsl.2019.115945

Crutchley, G. J., Kroeger, K. F., Pecher, I. A., & Gorman, A. R. (2018). How tectonic folding influences gas hydrate formation: New Zealand's Hikurangi subduction margin. *Geology*, *47*(1), 39–42. https://doi.org/10.1130/g45151.1

Crutchley, G. J., Maslen, G., Pecher, I. A., & Mountjoy, J. J. (2016). High-resolution seismic velocity analysis as a tool for exploring gas hydrate systems: An example from New Zealand's southern Hikurangi margin. *Interpretation*, *4*(1), SA1–SA12. https://doi.org/10.1190/INT-2015-0042.1

Davidson, S. R., Barnes, P. M., Pettinga, J. R., Nicol, A., Mountjoy, J.J., & Henrys, S. A. (2020). Conjugate strike-slip faulting across a subduction front driven by incipient seamount subduction. *Geology*, *48*(5), 493–498. https://doi.org/10.1130/G47154.1

Davis, D., Suppe, J., & Dahlen, F. A. (1983). Mechanics of fold-and- thrust belts and accretionary wedges. *Journal of Geophysical Research*, *88*(B2), 1153–1172. https://doi.org/10.1029/JB088iB02p01153

Davy, B., Hoernle, K., & Werner, R. (2008). Hikurangi Plateau: Crustal structure, rifted formation, and Gondwana subduction history. *Geochemistry, Geophysics, Geosystems*, *9*(7). https://doi.org/10.1029/2007GC001855

Dean, S. M., McNeill, L. C., Henstock, T. J., Bull, J. M., Gulick, S. P. S., Austin, J. A., et al. (2010). Contrasting décollement and prism properties over the Sumatra 2004–2005 earthquake rupture boundary. *Science*, *329*(5988), 207–210. https://doi.org/10.1126/science.1189373

Dominguez, S., Lallemand, S. E., Malavieille, J., & Von Huene, R. (1998). Upper plate deformation associated with seamount subduction. *Tectonophysics*, *293*(3–4), 207–224. https://doi.org/10.1016/S0040-1951(98)00086-9

Ellis, S., Ghisetti, F., Barnes, P. M., Boulton, C., Fagereng, Å., & Buiter, S. (2019). The contemporary force balance in a wide accretionary wedge: Numerical models of the southcentral Hikurangi margin of New Zealand. *Geophysical Journal International*, *219*(2), 776–795. https://doi.org/10.1093/gji/ggz317

Erslev, E. A. (1991). Trishear fault-propagation folding. *Geology*, *19*(6), 617–620. https://doi.org/10.1130/0091-7613(1991)019<0617:TFPF>2.3.CO;2

Fagereng, Å., & Toy, V. G. (2011). *Geology of the earthquake source: An introduction* (Vol. 359, pp. 1–16). Geological Society, London, Special Publications. https://doi.org/10.1144/SP359.1

Furlong, K. P., & Herman, M. (2017). Reconciling the deformational dichotomy of the 2016 M w 7.8 Kaikoura New Zealand earthquake. *Geophysical Research Letters*, *44*(13), 6788–6791. https://doi.org/10.1002/2017GL074365

Gase, A. C., Bangs, N. L., Van Avendonk, H. J. A., Bassett, D., & Henrys, S. A. (2022). Hikurangi megathrust slip behavior influenced by lateral variability in sediment subduction. *Geology*, *50*(10), 1145–1149. https://doi.org/10.1130/G50261.1

Gase, A. C., Van Avendonk, H. J. A., Bangs, N. L., Bassett, D., Henrys, S. A., Barker, D. H. N., et al. (2021). Crustal structure of the northern hikurangi margin, New Zealand: Variable accretion and overthrusting plate strength influenced by rough subduction. *Journal of Geophysical Research: Solid Earth*, *126*(5). https://doi.org/10.1029/2020JB021176

Geersen, J., McNeill, L., Henstock, T. J., & Gaedicke, C. (2013). The 2004 Aceh-Andaman Earthquake: Early clay dehydration controls shallow seismic rupture. *Geochemistry, Geophysics, Geosystems*, *14*(9), 3315–3323. https://doi.org/10.1002/ggge.20193

Ghisetti, F. C., Barnes, P. M., Ellis, S., Plaza-Faverola, A. A., & Barker, D. H. N. (2016). The last 2 Myr of accretionary wedge construction in the central Hikurangi margin (North Island, New Zealand): Insights from structural modeling. *Geochemistry, Geophysics, Geosystems*, *17*(7), 2661–2686. https://doi.org/10.1002/2016GC006341

Gibbs, A. D. (1983). Balanced cross-section construction from seismic sections in areas of extensional tectonics. *Journal of Structural Geology*, *5*(2), 153–160. https://doi.org/10.1016/0191-8141(83)90040-8

Gulick, S. P. S. S., Meltzer, A. M., & Clarke, S. H. (1998). Seismic structure of the southern Cascadia subduction zone and accretionary prism north of the Mendocino triple junction. *Journal of Geophysical Research*, *103*(B11), 27207–27222. https://doi.org/10.1029/98JB02526

Hamling, I. J., Hreinsdóttir, S., Clark, K., Elliott, J., Liang, C., Fielding, E., et al. (2017). Complex multifault rupture during the 2016 Mw 7.8 Kaikōura earthquake, New Zealand. *Science*, *356*(6334). https://doi.org/10.1126/science.aam7194

Han, S., Bangs, N. L., Carbotte, S. M., Saffer, D. M., & Gibson, J. C. (2017). Links between sediment consolidation and Cascadia megathrust slip behaviour. *Nature Geoscience*, *10*(12), 954–959. https://doi.org/10.1038/s41561-017-0007-2

Heuret, A., Conrad, C. P., Funiciello, F., Lallemand, S., & Sandri, L. (2012). Relation between subduction megathrust earthquakes, trench sediment thickness and upper plate strain. *Geophysical Research Letters*, *39*(5), 1–6. https://doi.org/10.1029/2011GL050712

Hossack, J. R. (1979). The use of balanced cross-sections in the calculation of orogenic contraction; a review. *Journal of the Geological Society*, *136*(6), 705–711. https://doi.org/10.1144/gsjgs.136.6.0705

Howarth, J. D., Orpin, A. R., Kaneko, Y., Strachan, L. J., Nodder, S. D., Mountjoy, J. J., et al. (2021). Calibrating the marine turbidite palaeo-seismometer using the 2016 Kaikōura earthquake. *Nature Geoscience*, *14*(3), 161–167. https://doi.org/10.1038/s41561-021-00692-6

Hughes, A. N., & Shaw, J. H. (2014). Fault displacement-distance relationships as indicators of contractional fault-related folding style. *AAPG Bulletin*, *98*(2), 227–251. https://doi.org/10.1306/05311312006

Hughes, A. N., & Shaw, J. H. (2015). Insights into the mechanics of fault-propagation folding styles. *Bulletin of the Geological Society of America*, *127*(11–12), 1752–1765. https://doi.org/10.1130/B31215.1

King, P. R. (2000). Tectonic reconstructions of New Zealand: 40 Ma to the present. *New Zealand Journal of Geology and Geophysics*, *43*(4), 611–638. https://doi.org/10.1080/00288306.2000.9514913

Kopp, H. (2013). Invited review paper: The control of subduction zone structural complexity and geometry on margin segmentation and seismicity. *Tectonophysics*, *589*, 1–16. https://doi.org/10.1016/j.tecto.2012.12.037

Kopp, H., & Kukowski, N. (2003). Backstop geometry and accretionary mechanics of the Sunda margin. *Tectonics*, *22*(6). https://doi.org/10.1029/2002TC001420

Kopp, H., Weinrebe, W., Ladage, S., Barckhausen, U., Klaeschen, D., Flueh, E. R., et al. (2008). Lower slope morphology of the Sumatra trench system. *Basin Research*, *20*(4), 519–529. https://doi.org/10.1111/j.1365-2117.2008.00381.x

Kroeger, K. F., Crutchley, G. J., Hillman, J. I., Turco, F., & Barnes, P. M. (2022). Gas hydrate formation beneath thrust ridges: A test of concepts using 3D modelling at the southern hikurangi margin, New Zealand. *Marine and Petroleum Geology*, *135*, 105394. https://doi.org/10.1016/j.marpetgeo.2021.105394

Lackey, J. K., Regalla, C. A., & Moore, G. F. (2020). Tectonic influences on trench slope basin development via structural restoration along the outer Nankai accretionary prism, southwest Japan. *Geochemistry, Geophysics, Geosystems*, *21*(8). https://doi.org/10.1029/2020GC009038

Laigle, M., Becel, A., De Voogd, B., Sachpazi, M., Bayrakci, G., Lebrun, J. F., & Evain, M. (2013). Along-arc segmentation and interaction of subducting ridges with the Lesser Antilles Subduction forearc crust revealed by MCS imaging. *Tectonophysics*, *603*, 32–54. https://doi.org/10.1016/j.tecto.2013.05.028

Laird, M. G., & Bradshaw, J. D. (2004). The break-up of a long-term relationship: The Cretaceous separation of New Zealand from Gondwana. *Gondwana Research*, *7*(1), 273–286. https://doi.org/10.1016/S1342-937X(05)70325-7

Lallemand, S. E., Malavieille, J., & Calassou, S. (1992). Effects of oceanic ridge subduction on accretionary wedges: Experimental modeling and marine observations. *Tectonics*, *11*(6), 1301–1313. https://doi.org/10.1029/92TC00637

Lee, J. M., Begg, J. G., & Forsyth, P. J. (2002). *Geology of the Wairarapa area*. Institute of Geological & Nuclear Sciences.

Lewis, K. B., Collot, J. Y., & Lallemand, S. E. (1998). The dammed Hikurangi Trough: A channel-fed trench blocked by subducting seamounts and their wake avalanches (New Zealand-France GeodyNZ project). *Basin Research*, *10*(4), 441–468. https://doi.org/10.1046/j.1365-2117.1998.00080.x

Lewis, K. B., & Pantin, H. M. (2002). Channel-axis, overbank and drift sediment waves in the southern Hikurangi Trough, New Zealand. *Marine Geology*, *192*(1–3), 123–151. https://doi.org/10.1016/S0025-3227(02)00552-2

Lewis, K. B., & Pettinga, J. R. (1993). The emerging, imbricate frontal wedge of the Hikurangi margin: Sedimentary basins of the world, *2*, 225–250.

MacKay, M. E., Moore, G. F., Cochrane, G. R., Casey Moore, J., & Kulm, L. V. D. (1992). Landward vergence and oblique structural trends in the Oregon margin accretionary prism: Implications and effect on fluid flow. *Earth and Planetary Science Letters*, *109*(3–4), 477–491. https://doi.org/10.1016/0012-821X(92)90108-8

Mackay, K. (2023). Bathymetric elevation models of the southern hikurangi subduction margin, New Zealand. [Dataset]. *Zenodo*. https://doi.org/10.5281/zenodo.10359823

McArthur, A. D., & Tek, D. E. (2021). Controls on the origin and evolution of deep-ocean trench-axial channels. *Geology*, *49*(8), 883–888. https://doi.org/10.1130/G48612.1

McNeill, L. C., Dugan, B., Petronotis, K. E., Backman, J., Bourlange, S., Chemale, F., et al. (2017). Expedition 362 summary. *Proceedings of the International Ocean Discovery Program*, *362*, 21–22. https://doi.org/10.7289/V5C8276M

McNeill, L. C., & Henstock, T. J. (2014). Forearc structure and morphology along the Sumatra-Andaman subduction zone. *Tectonics*, *33*(2), 112–134. https://doi.org/10.1002/2012tc003264

MGL1801 participants. (2018). The NZ3D experiment—Adding a new dimension for understanding slow slip events. *GeoPRISMS Newsletter*, *40*, 14–15.

Micallef, A., Mountjoy, J. J., Barnes, P. M., Canals, M., & Lastras, G. (2014). Geomorphic response of submarine canyons to tectonic activity: Insights from the Cook Strait canyon system, New Zealand. *Geosphere*, *10*(5), 905–929. https://doi.org/10.1130/GES01040.1

Midland Valley. (2014). MOVE software [software]. Midland Valley. Retrieved from http://www.mve.com

Moeremans, R., Singh, S. C., Mukti, M., McArdle, J., & Johansen, K. (2014). Seismic images of structural variations along the deformation front of the Andaman-Sumatra subduction zone: Implications for rupture propagation and tsunamigenesis. *Earth and Planetary Science Letters*, *386*, 75–85. https://doi.org/10.1016/j.epsl.2013.11.003

Moore, G. F., Park, J. O., Bangs, N. L., Gulick, S. P., Tobin, H., Nakamura, Y., et al. (2009). Structural and seismic stratigraphic framework of the NanTroSEIZE Stage 1 transect. *IODP Proceedings*, *314*. https://doi.org/10.2204/iodp.proc.314315316.102.2009

Moore, G. F., Saffer, D., Studer, M., & Costa Pisani, P. (2011). Structural restoration of thrusts at the toe of the Nankai Trough accretionary prism off Shikoku Island, Japan: Implications for dewatering processes. *Geochemistry, Geophysics, Geosystems*, *12*(5). https://doi.org/10.1029/2010GC003453

Moore, G. F., Shipley, T. H., Stoffa, P. L., Karig, D. E., Taira, A., Kuramoto, S., et al. (1990). Structure of the Nankai Trough accretionary zone from multichannel seismic reflection data. *Journal of Geophysical Research*, *95*(B6), 8753–8765. https://doi.org/10.1029/JB095iB06p08753

Moore, J. C., Mascle, A., Taylor, E., Andreieff, P., Alvarez, F., Barnes, R., et al. (1988). Tectonics and hydrogeology of the northern Barbados ridge: Results from ocean drilling program leg. *Bulletin of the Geological Society of America*, *100*, 1578–1593. https://doi.org/10.1130/0016-7606(1988)100<1578:TAHOTN>2.3.CO;2

Moore, J. C., & Saffer, D. (2001). Updip limit of the seismogenic zone beneath the accretionary prism of Southwest Japan: An effect of diagenetic to low-grade metamorphic processes and increasing effective stress. *Geology*, *29*(2), 183–186. https://doi.org/10.1130/0091-7613(2001)029<0183:ULOTSZ>2.0.CO;2

Morgan, J. K., & Karig, D. E. (1995). Decollement processes at the Nankai accretionary margin, southeast Japan: Propagation, deformation, and dewatering. *Journal of Geophysical Research*, *100*(B8), 15221–15231. https://doi.org/10.1029/95jb00675

Mortimer, N. (2004). New Zealand's geological foundations. *Gondwana Research*, *7*(1), 261–272. https://doi.org/10.1016/S1342-937X(05)70324-5

Mountjoy, J. J., & Barnes, P. M. (2011). Active upper plate thrust faulting in regions of low plate interface coupling, repeated slow slip events, and coastal uplift: Example from the Hikurangi Margin, New Zealand. *Geochemistry, Geophysics, Geosystems*, *12*, 1. https://doi.org/10.1029/2010GC003326

Mountjoy, J. J., Barnes, P. M., & Pettinga, J. R. (2009). Morphostructure and evolution of submarine canyons across an active margin: Cook Strait sector of the Hikurangi Margin, New Zealand. *Marine Geology*, *260*(1–4), 45–68. https://doi.org/10.1016/j.margeo.2009.01.006

Mountjoy, J. J., Howarth, J. D., Orpin, A. R., Barnes, P. M., Bowden, D. A., Rowden, A. A., et al. (2018). Earthquakes drive large-scale submarine canyon development and sediment supply to deep-ocean basins. *Science Advances*, *4*(3). https://doi.org/10.1126/sciadv.aar3748

Mouslopoulou, V., Saltogianni, V., Nicol, A., Oncken, O., Begg, J., Babeyko, A., et al. (2019). Breaking a subduction-termination from top to bottom: The large 2016 Kaikōura Earthquake, New Zealand. *Earth and Planetary Science Letters*, *506*, 221–230. https://doi.org/10.1016/j.epsl.2018.10.020

Nicol, A., & Beavan, J. (2003). Shortening of an overriding plate and its implications for slip on a subduction thrust, central Hikurangi Margin, New Zealand. *Tectonics*, *22*(6). https://doi.org/10.1029/2003TC001521

Nicol, A., Mazengarb, C., Chanier, F., Rait, G., Uruski, C., & Wallace, L. (2007). Tectonic evolution of the active Hikurangi subduction margin, New Zealand, since the Oligocene. *Tectonics*, *26*(4). https://doi.org/10.1029/2006TC002090

Pedley, K. L., Barnes, P. M., Pettinga, J. R., & Lewis, K. B. (2010). Seafloor structural geomorphic evolution of the accretionary frontal wedge in response to seamount subduction, Poverty Indentation, New Zealand. *Marine Geology*, *270*(1–4), 119–138. https://doi.org/10.1016/j.margeo.2009.11.006

PEG09. (2009). New Zealand Petroleum and Minerals. [Dataset] (p. PR4158). Retrieved from https://geodata.nzpam.govt.nz/survey/1192170815

Petrel. (2019). *[Software] SLB*. Retrieved from https://www.slb.com/products-and-services/delivering-digital-at-scale/software/petrel-subsurface-software/petrel

Pizer, C., Clark, K., Howarth, J., Garrett, E., Wang, X., Rhoades, D., & Woodroffe, S. (2021). Paleotsunamis on the southern hikurangi subduction zone, New Zealand. *Show Regular Recurrence of Large Subduction Earthquakes: The Seismic Record*, *1*(2), 75–84. https://doi.org/10.1785/0320210012

Plaza-Faverola, A., Henrys, S., Pecher, I., Wallace, L., & Klaeschen, D. (2016). Splay fault branching from the Hikurangi subduction shear zone: Implications for slow slip and fluid flow. *Geochemistry, Geophysics, Geosystems*, *17*(12), 5009–5023. https://doi.org/10.1002/2016GC006563

Plaza-Faverola, A., Klaeschen, D., Barnes, P., Pecher, I., Henrys, S., & Mountjoy, J. (2012). Evolution of fluid expulsion and concentrated hydrate zones across the southern Hikurangi subduction margin, New Zealand: An analysis from depth migrated seismic data. *Geochemistry, Geophysics, Geosystems*, *13*(8). https://doi.org/10.1029/2012GC004228

Rait, G., Chanier, F., & Waters, D. W. (1991). Landward- and seaward-directed thrusting accompanying the onset of subduction beneath New Zealand. *Geology*, *19*(3), 230–233. https://doi.org/10.1130/0091-7613(1991)019<0230:LASDTA>2.3.CO;2

Rattenbury, M. S., Townsend, D. B., & Johnston, M. R. (2006). *Geology of the Kaikoura area. Institute of geological & Nuclear sciences 1:250 000 geological map 13. 1 sheet + 70 p. Lower Hutt, New Zealand*. GNS Science. (compilers).

Riefstahl, F., Gohl, K., Davy, B., & Barrett, R. (2020). Extent and cessation of the mid-Cretaceous Hikurangi Plateau underthrusting: Impact on global plate tectonics and the submarine Chatham Rise. *Journal of Geophysical Research: Solid Earth*, *125*(8). https://doi.org/10.1029/2020JB019681

RPS Energy. (2010). *Pegasus Basin, bounty trough and SAHKE seismic—Report on contractor's performance during 2D seismic survey 13th November 2009 to 30th March 2010*. Ministry of Economic Development New Zealand Unpublished Petroleum Report PR 4158.

Saffer, D. M., & Bekins, B. A. (2002). Hydrologic controls on the mechanics and morphology of accretionary wedges and thrust belts. *Geology*, *30*(3), 271–274. https://doi.org/10.1130/0091-7613(2002)030<0271:HCOTMA>2.0.CO;2

Seebeck, H., Van Dissen, R., Litchfield, N., Barnes, P. M., Nicol, A., Langridge, R., et al. (2023). The New Zealand Community fault model–version 1.0: An improved geological foundation for seismic hazard modelling. *New Zealand Journal of Geology and Geophysics*, *67*(2), 209–229. https://doi.org/10.1080/00288306.2023.2181362

Shipley, T. H., & Moore, G. F. (1986). Sediment accretion, subduction, and dewatering at the base of the trench slope off Costa Rica: A seismic reflection view of the decollement (Pacific). *Journal of Geophysical Research*, *91*(B2), 2019–2028. https://doi.org/10.1029/JB091iB02p02019

Sibuet, J. C., Rangin, C., Lepichon, X., Singh, S., Cattaneo, A., Graindorge, D., et al. (2007). 26th December 2004 great Sumatra-Andaman earthquake: Co-Seismic and post-seismic motions in northern Sumatra. *Earth and Planetary Science Letters*, *263*(1–2), 88–103. https://doi.org/10.1016/j.epsl.2007.09.005

Smith, G., McNeill, L., Henstock, I. J., & Bull, J. (2012). The structure and fault activity of the Makran accretionary prism. *Journal of Geophysical Research*, *117*(B7), 1–17. https://doi.org/10.1029/2012JB009312

Stern, T. A., Stratford, W. R., & Salmon, M. L. (2006). Subduction evolution and mantle dynamics at a continental margin: Central North Island, New Zealand. *Reviews of Geophysics*, *44*(4). https://doi.org/10.1029/2005RG000171

Stevens, D. E., Henstock, T. J., & McNeill, L. C. (2021). Evolution of the thermal and dehydration state of sediments entering the North Sumatra Subduction Zone. *Geochemistry, Geophysics, Geosystems*, *22*(4). https://doi.org/10.1029/2020gc009306

Strogen, D. P., Seebeck, H., Hines, B. R., Bland, K. J., & Crampton, J. S. (2022). Palaeogeographic evolution of Zealandia: Mid-cretaceous to present. *New Zealand Journal of Geology and Geophysics*, *66*(3), 528–557. https://doi.org/10.1080/00288306.2022.2115520

Tavani, S., Storti, F., & Salvini, F. (2005). Rounding hinges to fault-bend folding: Geometric and kinematic implications. *Journal of Structural Geology*, *27*(1), 3–22. https://doi.org/10.1016/j.jsg.2004.07.005

Tek, D. E., McArthur, A. D., Poyatos-Moré, M., Colombera, L., Allen, C., Patacci, M., & McCaffrey, W. D. (2021). Controls on the architectural evolution of deep-water channel overbank sediment wave fields: Insights from the Hikurangi Channel, offshore New Zealand. *New Zealand Journal of Geology and Geophysics*, *65*(1), 141–178. https://doi.org/10.1080/00288306.2021.1978509

Tsuji, T., Ashi, J., & Ikeda, Y. (2014). Strike-slip motion of a mega-splay fault system in the Nankai oblique subduction zone. *Earth Planets and Space*, *66*(1), 120. https://doi.org/10.1186/1880-5981-66-120

Tsuji, T., Ashi, J., Strasser, M., & Kimura, G. (2015). Identification of the static backstop and its influence on the evolution of the accretionary prism in the Nankai Trough. *Earth and Planetary Science Letters*, *431*, 15–25. https://doi.org/10.1016/j.epsl.2015.09.011

Turco, F., Crutchley, G. J., Gorman, A. R., Mountjoy, J. J., Hillman, J. I. T., & Woelz, S. (2020). Seismic velocity and reflectivity analysis of concentrated gas hydrate deposits on the southern Hikurangi Margin (New Zealand). *Marine and Petroleum Geology*, *120*, 104572. https://doi.org/10.1016/j.marpetgeo.2020.104572

Underwood, M. B. (2007). Sediment inputs to subduction zones: Why lithostratigraphy and clay mineralogy matter. In T. H. Dixon & J. C. Moore (Eds.), *The seismogenic zone of subduction thrust faults* (pp. 42–85). Columbia University Press. https://doi.org/10.7312/dixo13866-003

Von Huene, R., Ranero, C. R., & Scholl, D. W. (2009). Convergent margin structure in high-quality geophysical images and current kinematic and dynamic models. In S. Lallemand & F. Funiciello (Eds.), *Convergent margin structure in high-quality geophysical images and current kinematic and dynamic models BT - subduction zone geodynamics* (pp. 137–157). Springer Berlin Heidelberg. https://doi.org/10.1007/978-3-540-87974-9_8

Von Huene, R., & Scholl, D. W. (1991). Observations at convergent margins concerning sediment subduction, subduction erosion, and the growth of continental crust. *Reviews of Geophysics*, *29*(3), 279–316. https://doi.org/10.1029/91RG00969

Wallace, L. M., Barnes, P., Beavan, J., Van Dissen, R., Litchfield, N., Mountjoy, J., et al. (2012). The kinematics of a transition from subduction to strike-slip: An example from the central New Zealand plate boundary. *Journal of Geophysical Research*, *117*(B2). https://doi.org/10.1029/2011JB008640

Wallace, L. M., & Beavan, J. (2010). Diverse slow slip behavior at the Hikurangi subduction margin, New Zealand. *Journal of Geophysical Research*, *115*(B12). https://doi.org/10.1029/2010JB007717

Wallace, L. M., Beavan, J., Bannister, S., & Williams, C. (2012). Simultaneous long-term and short-term slow slip events at the Hikurangi subduction margin, New Zealand: Implications for processes that control slow slip event occurrence, duration, and migration. *Journal of Geophysical Research B: Solid Earth*, *117*(B11). https://doi.org/10.1029/2012JB009489

Wallace, L. M., Beavan, J., McCaffrey, R., Berryman, K., & Denys, P. (2007). Balancing the plate motion budget in the South Island, New Zealand using GPS, geological and seismological datas. *Geophysical Journal International*, *168*(1), 332–352. https://doi.org/10.1111/j.1365-246X.2006.03183.x

Wallace, L. M., Beavan, J., McCaffrey, R., & Darby, D. (2004). Subduction zone coupling and tectonic block rotations in the North Island, New Zealand. *Journal of Geophysical Research*, *109*(B12), 1–21. https://doi.org/10.1029/2004JB003241

Wallace, L. M., Cochran, U. A., Power, W. L., & Clark, K. J. (2014). Earthquake and tsunami potential of the Hikurangi subduction thrust, New Zealand: Insights from paleoseismology, GPS, and Tsunami modeling. *Oceanography*, *27*(2), 104–117. https://doi.org/10.5670/oceanog.2014.46

Wallace, L. M., Hreinsdóttir, S., Ellis, S., Hamling, I., D'Anastasio, E., & Denys, P. (2018). Triggered slow slip and afterslip on the southern hikurangi subduction zone following the Kaikōura earthquake. *Geophysical Research Letters*, *45*(10), 4710–4718. https://doi.org/10.1002/2018GL077385

Wallace, L. M., Reyners, M., Cochran, U., Bannister, S., Barnes, P. M., Berryman, K., et al. (2009). Characterizing the seismogenic zone of a major plate boundary subduction thrust: Hikurangi Margin, New Zealand. *Geochemistry, Geophysics, Geosystems*, *10*. https://doi.org/10.1029/2009GC002610

Wallace, L. M., Saffer, D. M., Barnes, P. M., Pecher, I. A., Petronotis, K. E., & LeVay, L. J. (2019). *Expedition 372/375 Scientists, 2019, Hikurangi subduction margin coring, logging, and observatories: Proceedings of the International Ocean Discovery Program, volume 372B/375*. International Ocean Discovery Program.

Wang, T., Wei, S., Shi, X., Qiu, Q., Li, L., Peng, D., et al. (2018). The 2016 Kaikōura earthquake: Simultaneous rupture of the subduction interface and overlying faults. *Earth and Planetary Science Letters*, *482*, 44–51. https://doi.org/10.1016/j.epsl.2017.10.056

Watson, S. J., Mountjoy, J. J., Barnes, P. M., Crutchley, G. J., Lamarche, G., Higgs, B., et al. (2020). Focused fluid seepage related to variations in accretionary wedge structure, hikurangi margin, New Zealand. *Geology*, *48*(1), 56–61. https://doi.org/10.1130/G46666.1

Westbrook, G. K., Smith, M. J., Peacock, J. H., & Poulter, M. J. (1982). Extensive underthrusting of undeformed sediment beneath the accretionary complex of the Lesser Antilles subduction zone. *Nature*, *300*(5893), 625–628. https://doi.org/10.1038/300625a0

Wood, R., & Davy, B. (1994). The Hikurangi Plateau. *Marine Geology*, *118*(1–2), 153–173. https://doi.org/10.1016/0025-3227(94)90118-X